Vitamin D_3/Vitamin K_2/Magnesium-Loaded Polylactic Acid/Tricalcium Phosphate/Polycaprolactone Composite Nanofibers Demonstrated Osteoinductive Effect by Increasing Runx2 via Wnt/B-Catenin Pathway

Ece Guler[1,2,a], Yaren Ezgi Baripoglu[3,a], Hussain Alenezi[4,5], Ayca Arikan[3], Ravana Babazade[1,2], Semra Unal[2], Gokhan Duruksu[6], Fawzan S. Alfares[5], Yusufhan Yazir[6], Faik Nuzhet Oktar[2,7], Oguzhan Gunduz[2,8], Mohan Edirisinghe[2,4], Muhammet Emin Cam[1,2*]

[1]Department of Pharmacology, Faculty of Pharmacy, Marmara University, Istanbul 34854, Turkey

[2]Center for Nanotechnology and Biomaterials Application and Research, Marmara University, Istanbul 34722, Turkey

[3]Department of Bioengineering, Faculty of Technology, Marmara University, Istanbul 34722, Turkey

[4]Department of Mechanical Engineering, University College London, Torrington Place, London WC1E 7JE, UK

[5]Department of Manufacturing Engineering, College of Technological Studies, PAAET, 13092 Kuwait City, Kuwait

[6]Stem Cell and Gene Therapies Research and Applied Center, Medical Faculty, Kocaeli University, Kocaeli 41380, Turkey

[7]Department of Bioengineering, Faculty of Engineering, Marmara University, 34722, Turkey

[8]Department of Metallurgy and Material Engineering, Faculty of Technology, Marmara University, Istanbul 34722, Turkey

[a]Contributed equally to this work

*Corresponding Author (Muhammet Emin Cam); Postal address: Department of Pharmacology,

Faculty of Pharmacy, Marmara University, Istanbul 34854, Turkey; Tel: +90 216 777 52 00;
Fax: +90 216 777 52 01
E-mail addresses: muhammet.cam@marmara.edu.tr

ABSTRACT

Vitamin D_3, vitamin K_2, and Mg (10%, 1.25%, and 5%, w/w, respectively)-loaded PLA (12%, w/v) (TCP (5%, w/v)) / PCL (12%, w/v) 1:1 (v/v) composite nanofibers (DKMF) were produced by electrospinning method (ES) and their osteoinductive effects were investigated in cell culture test. Neither pure nanofibers nor DKMF caused a significant cytotoxic effect in fibroblasts. The induction of the stem cell differentiation into osteogenic cells was observed in the cell culture with both DKMF and pure nanofibers, separately. Vitamin D_3, vitamin K_2, and magnesium demonstrated to support the osteogenic differentiation of mesenchymal stem cells by expressing Runx2, BMP2, and osteopontin and suppressing PPAR-γ and Sox9. Therefore, the Wnt/β-Catenin signalling pathway was activated by DKMF. DKMF promoted large axonal sprouting and needle-like elongation of osteoblast cells and enhanced cellular functions such as migration, infiltration, proliferation, and differentiation after seven days of incubation using confocal laser scanning microscopy. The results showed that DKMF demonstrated sustained drug release for 144 h, tougher and softer structure, higher tensile strength, increased water up-take capacity, decreased degradation ratio, and slightly lower Tm and Tg values compared to pure nanofibers. Consequently, DKMF is a promising treatment approach in bone tissue engineering due to its osteoinductive effects.

Keywords: Bone tissue engineering; Composite nanofiber; Osteoblast cell

1. INTRODUCTION

Bone tissue engineering has been one of the fascinating areas with the development of technology. This area, which is the sub-branch of tissue engineering, targets regenerating or repairing bone by being interested in forming tissue and bone structure and mechanism. The bones are the most rigid tissues of the human body and provide a store for calcium, phosphorus, and other critical components of the hematopoietic system. Furthermore, they have also several different functions such as the production of blood cells, support, and movement.[1, 2]

Different treatment approaches have been applied to improve bone structure with the development of nanotechnology. Nanofibers are one of these approaches is used in the treatment of damaged bone tissues. The components in the structure of produced fibers have great importance in this treatment approach. The reason for that is that these composites affect several structural properties belong to fibers, such as being biocompatible and three dimensional, having proper mechanical properties, large surface area to volume ratio, and appropriate functionality.[3, 4]

Electrospinning (ES) is a common technique used to produce nanoscale and controllable fibers by using polymer solutions in a high electric field.[5] These nanofibers produced by ES is used for several tissue engineering applications such as bone, tendon, neural, and vascular. An ideal three-dimensional scaffold should structurally mimic the bulk tissue, but also the bone healing process should mechanically be supported, and biochemical improvements should be provided to induce osteogenesis. ES is one of the ideal techniques in order to fabricate ideal three-dimensional scaffolds for bone tissue engineering.[6, 7]

Polylactic acid (PLA) is an FDA approved biodegradable biopolymer, which is produced from renewable sources. PLA provides mechanical strength and integrity to the fibers.[8] Tricalcium phosphate (TCP) is a porous ceramic and a soluble form of calcium phosphate, which can degrade and release Ca^{2+} and PO_4^{3-} into the environment. Several studies have shown that electrospun materials with calcium phosphate have low cytotoxicity, high cellular proliferation,

and high mineralization.[9] TCP can also be used as a tissue replacement or combined with other polymers. Polycaprolactone (PCL) is also an FDA approved biocompatible and biodegradable polymer and has some different properties such as easy availability, cost-efficacy, and suitability for modification. PCL is compatible with hard and soft tissue materials, and it is suitable for thermoplastic processing, cartilage, and bone repairment in tissue engineering applications. It is especially suitable for bone tissue engineering applications because of its biological properties, adjustable physicochemical state, and distinct mechanical and chemical properties.[10] It has better potential for making implantable devices because of its slower rate of degradation, which is better than other polylactides.[11]

Vitamin D is an oil-soluble crucial vitamin for human health and consists of two major forms, vitamin D_2 and vitamin D_3 (D_3).[12] D_3 is an active form of vitamin D for human and helps to protect the healthy skeleton. The primary function of D_3 is to maintain concentrations of serum phosphorus and calcium within the normal range to protect essential cellular functions and encourage mineralization of the skeleton either directly by controlling calcium absorption in the intestine or indirectly influence osteoblasts.[13] It allows calcium to be sufficiently absorbed in the gut and used by the body. Vitamin D deficiency is one of the most important health problems globally in all age groups because of it leading to different diseases, increased bone resorption and decreased calcium absorption. Therefore, recent studies target to improve the bioavailability and bioactivity of vitamin D_3 by using different drug delivery systems. [14, 15]

Vitamin K is one of the oil-soluble vitamins consisting of three forms: the most well-known vitamin K_1, vitamin K_2 (K_2), and unnatural vitamin K_3 and the structural difference between them are their substituent R groups. Vitamin K_1 and K_2 are essential to maintain blood hemostasis, heart and bone health. They play a vital role in optimizing the calcium used in the body. Especially K_2 is necessary for calcium usage and inhibits arterial calcification, and helps strengthen the bones. Several studies demonstrate that K_2 also prevents bone loss related to

ageing. In addition, it has a protective effect for bones due to its promotion of osteoblast differentiation and mineralization. [16, 17]

Magnesium (Mg) is the second most abundant mineral and an intracellular cation contributing to bone stabilization, bone growth, and mineralization. Mg, which affects both matrix and mineral metabolism in bone, is chosen due to its biocompatibility, biodegradation, and role in several processes. Recent studies have shown that Mg has a crucial function in skeletal development and bone remodeling due to its osteogenesis and angiogenesis functions. Furthermore, it was found that Mg increases the wound healing process and decreases the healing time. [18, 19]

In this study, PLA, PCL, and TCP have been used as the polymer in the production of PLA(TCP)/PCL composite nanofibers produced using ES due to their essential properties, biocompatibility, biodegradability, and mechanical strength. The active pharmaceutical ingredients (APIs), which are D_3, K_2, and Mg, are essential for bone repairment and regeneration, were loaded in nanofibers and physical parameter tests of solutions, SEM, FTIR, XRD, DSC, tensile strength, encapsulation efficiency, drug release tests, WST, and also cell culture test were performed to investigate the osteoinductive effects of produced nanofibers for bone tissue engineering.

2.MATERIALS AND METHODS

2.1. Materials

Poly (L-lactic acid) (PLA) 2003D, poly (caprolactone) (PCL, Mw~80,000), tricalcium phosphate (TCP, Mw ~310.18 g/mol), other reagents, e.g., chloroform, N,N-dimethylformamide (DMF), methanol and all the APIs, e.g., magnesium, vitamin D_3, vitamin K_2 were supplied from Sigma-Aldrich (Poole, UK).

2.2. Methods

2.2.1. Preparation of Solutions

3.6 g PLA and 1.5 g TCP were dissolved in 30 mL chloroform/DMF (3:1, v/v) to prepare PLA (12%, w/v)/TCP (5%, w/v) solution and stirred for approximately 2.5 h. 3.6 g PCL was dissolved

130 in 30 mL chloroform/methanol (3:1, v/v) solution, prepared 12% (w/v) PCL solution by stirring
131 for approximately 1 h. PLA(TCP) and PCL were blended at three different ratios (3:1, 1:1, 1:3,
132 v/v).
133 145 mg Magnesium, 18.1 mg D_3, and 72.5 mg K_2 were dissolved in 30 mL PLA (TCP)/PCL
134 (1:1, w/v) to be at concentrations of 10% [18], 1.25% [20], and 5%, respectively. Vitamin K_2
135 was dissolved in PLA (TCP)/PCL solution at the maximum possible level. All procedures were
136 carried out at room temperature. Physical parameters such as electrical conductivity, density,
137 viscosity, and surface tension of the solutions were measured by using a standard density bottle
138 (10 ml, Boru Cam Inc., Turkey), the electrical conductivity probe (Cond 3110 SET 1, WTW,
139 Germany.), a force tensiometer (Sigma 703D, Attension, Germany), and a viscometer (DV-E,
140 Brookfield AMETEK, USA), respectively. All the measurements were repeated three times at
141 ambient temperature.
142 **2.2.2. Electrospinning Process**
143 ES apparatus contains a syringe pump, in which is put the polymer solution (NE-300, New Era
144 Pump Systems, Inc., USA), a single needle, a high voltage generator that connects with the
145 needle, and a laboratory-scale electrospinning unit (NS24, Inovenso Co., Turkey). The applied
146 voltage was fixed to 25.0 kV and the distance between the needle tip and the collector was set to
147 150 mm for all pure fibers. The flow rates were set to 0.08 mL/h, 0.1 mL/h, and 0.18 mL/h for
148 1:1, 3:1, and 1:3 (v/v) PLA(TCP)/PCL ratios, respectively. According to SEM results,
149 PLA(TCP)/PCL at 1:1 (v/v) ratio was selected as the optimized ratio.
150 APIs were added to the 1:1 (v/v) ratio of PLA(TCP)/PCL solution, and the voltage and flow rate
151 was set to 24 kV and 0.38 mL/h, respectively. The distance between the needle tip and the
152 collector was set to 200 mm.
153 **2.2.3. Scanning Electron Microscopy (SEM)**
154 SEM (EVO LS 10, ZEISS) was used to investigate the size and morphology of fibers. The
155 surface of the samples was coated with gold for the 60s. The applied accelerating voltage was 20

kV and the working distance was 25 mm. Image software (Brocken Symmetry Software) was used to determine the mean diameter and distribution of fibers.

2.2.4. Fourier Transforms Infrared Spectroscopy (FTIR)

FTIR (Jasco, FT/IR 4700) was used to analyze the molecular content of the fibers. Measurements were carried out at room temperature (23°C) in the transmission mode over the range 500-4000 cm^{-1} with a resolution of 4 cm^{-1}. OPUS Viewer version 6.5 software was used until the end of the analysis.

2.2.5. X-ray Powder Diffraction (XRD)

XRD was performed using a D/Max-BR diffractometer (RigaKu, Tokyo, Japan) to examine the crystalline form and structure of the fibers. Analyses were carried out at 40 mV and 30 mA over a 2θ range of 5-90 ^{o} at a rate of 2 ^{o}/min. In order to converse the obtained data to diffractograms, OriginPro 7.0 software (OriginLab Corporation, MA, USA) was used.

2.2.6. Differential Scanning Calorimetry (DSC)

DSC was performed to determine the thermal properties of the fibers by using Perkin Elmer Jade DSC and Pyris software (PerkinElmer Inc., Mass., USA). The heating rate was 10 ^{o}C min^{-1} between 0 and 200 ^{o}C under a dynamic argon atmosphere (20 mL min^{-1}). Temperature calibration of DSC was carried out according to the indium melting point and melting enthalpy. Perkin Elmer aluminum sample pans and covers were utilized. Samples of approximately 7.0 mg of mass were placed in the pan and crimped before the measurements; peak temperature of endotherms was considered as melting temperature. Tg values were determined at half the height of the displacement.

2.2.7. Tensile Test

Instron 4411 tensile machine was used to measure the tensile strength of the fiber samples at room temperature (23 ^{o}C). Bluehill 2 software (Elancourt, France) was used to examine the results. Fibers were tested, and a digital micrometer (Mitutoyo MTI Corp., USA) was utilized to determine the thickness of the fibers. The top and bottom of the grip compressed both ends of the

fibers, and the tensile test was carried out under 5 mm min^{-1} test speed and 10 mm distance between grips. Three samples were taken from each fiber sample (10x50 mm) for the tensile test.

2.2.8. Drug Encapsulation Efficiency

The mass of actual APIs loaded in nanofibers/mass of APIs used in nanofibers fabrication is defined as encapsulation efficiency (EE). Standard procedure was used to define the content of D_3, K_2, and Mg in fibers. Firstly, the fibers were completely dissolved in their solvent mixes, and detections for D_3, K_2, and Mg were carried out with UV at 296 nm[21], 248 nm[22], and 215 nm[23], respectively. D_3/K_2/Mg-loaded fibers (DKMF) were weighed an average amount of 5 mg each and dissolved in a vial by adding a 10 ml solvent mixture. The vials were gently mixed for 1.5 hours to completely release D_3, K_2, and Mg from fibers to solvent mixtures. 1 ml of each solution was taken and detected using a UV-visible spectrophotometer (Shimadzu UV-3600, Japan). All measurements were repeated three times for all three solutions.

2.2.9. *In Vitro* Drug Release

Firstly, D_3, K_2, and Mg solutions were separately prepared with phosphate-buffered saline (PBS) containing Tween 80 (0.5%, w/v) at five different concentrations (0.2, 0.4, 0.6, 0.8, and 1 µg/ml) to create a linear calibration curve for each one. This analysis was performed to investigate the release properties of D_3, K_2, and Mg from DKMF. Nanofibers were cut approximately 5 mg in weight and then immersed in 1 mL of PBS (pH 7.4 at 37°C) containing Tween 80 (0.5%, w/v). After that, they were held on a rotary shaker at 250 rpm, 37 °C during the test process. 1 ml PBS containing Tween 80 (0.5%, w/v) was taken from DKMF samples at scheduled times (0, 0.25, 0.5, 1, 2, 3, 4, 6, 8, 12, 24, 48, 72, 96, 120, and 144h) and 1 mL of fresh PBS containing Tween 80 (0.5%, w/v) was added to the Eppendorf vials to continue the drug release test. Tween 80 was added to PBS in order to increase the solubility of D_3 and K_2[24]. UV spectroscopy (Shimadzu UV-3600, Japan) was used to analyze the release profiles of D_3, K_2, and Mg at 252 nm, 271 nm, 255 nm, respectively.

2.2.10. *In Vitro* Drug Release Kinetics

Five different mathematical models were used to analyze the drug release kinetics from DKMF. These kinetic models are zero-order, first-order, and Hixson Crowell models.[25] The equations belong to zero-order (1), first-order (2), and Hixson-Crowell (3) models are as follows, respectively:

$$Q = K_0 t \quad (1)$$

$$Q ln\,(1 - Q) = -K_1 t \quad (2)$$

$$Q^{1/3} = K_{hc} t \quad (3)$$

In these equations, Q is the fractional amount of drug release at time t; K_0, K_1, and K_{hc} are the kinetic constants for zero-order, first-order, and Hixson-Crowell models, respectively. N is the diffusion exponent, which is indicative of the drug release mechanism.

2.2.11. *In Vitro* Degradation Test

The conventional methods were used for performing the degradation test of nanofibers. Briefly, each dried nanofibers were cut into small square pieces as being of the initial weight of ~5 mg. Firstly, they were immersed in 1 mL of HCl for an hour for simulating stomach acid, and then, it was continued with PBS (pH 7.4) in a 37 °C shaking incubator for up to 41 days. The fresh PBS solution as much as the used amount was added after each measurement. Samples were measured at 1, 4, 8, 12h, and on days 5, 9, 13, 17, 21, 24, 29, 33, 37, and 41. The water on the surface was gently removed by filter paper after the removal of the samples. After that, samples for each time point were dried in a vacuum dryer and subsequently weighed until a constant weight was obtained. The degradation of mass loss (%) was calculated as follows:

$$Degredation\ test\ (\%) = [(W_0 - W_t)/W_0]\ x\ 100$$

where W_0 is the original weight, and W_t is the weight of the degraded sample at incubation time (t).

2.2.12. *In Vitro* Swelling Test

The swelling behavior of nanofibers was evaluated by measuring the initial weight of the dry samples. After that, nanofibers were immersed in PBS (pH 7.4, 37 °C) for different periods intervals (0.5, 1, 2, 3, 8, 24h). Three replicates were performed for each sample. Before measuring the weight of the swollen samples, the water on the surface was gently removed by a filter paper. The swelling ratio was calculated using the following equation:

$$Swelling\ ratio\ (\%) = (W_t - W_0)/W_0\ x\ 100$$

where W_0 is the original weight, and W_t is the weight of the swollen sample at incubation time (t).

2.2.13. Cell Culture and Cytotoxicity Assay

The cytotoxicity of nanofibers was determined on fibroblast cells by WST-1 assay (Roche, Mannheim, Germany). Human fibroblast cells were seeded in 96-well plates at a density of 1.0×10^4 cells per well (n=6) and incubated in DMEM (Thermo, Gibco, Paisley, UK) supplemented with 10 % fetal bovine serum (FBS) (Thermo, Gibco) and %1 Pen-Strep (Thermo, Gibco) at 37 °C in a humidified atmosphere of 5 % CO_2 for 24 hours. 5 mm diameter circles from nanofibers were cut out and incubated for 24 hours at 37 °C in 200 µL DMEM without cell. For cytotoxicity assay, the normal culture medium was replaced with this 24-h-conditioned medium (supplemented with serum and antibiotics) and incubated for 48 hours at 37 °C in the humidified atmosphere of 5 % CO_2. Then, the medium was replaced with a 10 % WST-1 solution in DMEM, and the cells were incubated for 2 hours at 37 °C. The formation of the soluble formazan dye was measured at the wavelength of 450 nm using a spectrophotometer. The cell viability was expressed as a percentage of control cultures (cell culture in DMEM without the conditioning with nanofiber).

2.2.14. Stem Cell Differentiation Assay

Bone-marrow-derived mesenchymal stem cells (hBM-MSCs) derived from iliac crest bone marrow aspirates were used for osteogenic differentiation study.[26] The cells were previously

isolated and cryo-preserved at the KOGEM cell bank (Kocaeli University, Kocaeli, Turkey). hBM-MSCs were cultured in DMEM (Gibco) supplemented with 10% FBS and 1% penicillin-streptomycin under the standard culture condition at 37°C in a humidified atmosphere with 5% CO_2. After cells reached 70-80% confluency, cells were passaged by 0.25% trypsin-EDTA (Gibco). The effect of pure nanofibers or DKMF on hBM-MSCs was evaluated by the expression analyses of osteogenic differentiation markers (Runx2, osteopontin, BMP2), chondrogenic differentiation marker (Sox9), and adipogenic differentiation marker (PPAR-γ) after the 2-week culture in the normal (culture) medium or in the osteogenic differentiation medium (StemPro Osteogenesis Differentiation Kit, Thermo Fisher Scientific, Gibco, Grand Island, NY). The total RNA was extracted by Aurum Total RNA Mini Kit (Bio-Rad, Hercules, CA), and cDNA was synthesized by iScript cDNA Synthesis Kit (Biorad) using the protocol supplied by the manufacturer. The gene expression was evaluated using iTaq Universal SYBR Green Supermix (Biorad) in the LightCycler 480-II system (Roche). PCR amplification followed a two-step cycling program: 30 s pre-denaturation at 95 °C, 45 cycles of 95 °C for 15 s, and 60 °C for 60 s. Cp values were determined by LightCycler 480 Software (release 1.5). ActB gene amplification was used as a housekeeping gene in the calculations.

2.2.15. Cell morphology

On days 1, 3, and 7, after washing with ice-cold PBS two times, cell-loaded nanofibers were fixed with 2.5 % glutaraldehyde and then serial dilutions of ethanol (30-50-70-90 %) and dried in air. Images were collected with an acceleration voltage of 10 kV from gold-plated samples using SEM.

Cell infiltration into the nanofibers was observed under a confocal laser scanning microscope (Zeiss LSM700). After incubation period at 1, 3, and 7 days, the samples were washed with PBS, fixed with 4% formaldehyde for 1 h, and again washed with PBS. Permeabilization was then performed with 0.1% Triton X-100 in PBS for 15 min, followed by washing with PBS. The samples were incubated with FITC–phalloidin for 1 h at room temperature and washed with

PBS. The samples were then placed on glass slides using DAPI. The cell fluorescence was determined using a confocal laser scanning microscope with a 20x oil-immersion objective for image acquisition. The excitation wavelength for FITC was fixed at 488 nm, while the emission wavelength was set at 500–540 nm. On the other hand, the excitation and emission wavelengths for DAPI were fixed at 358 nm and 461 nm, respectively. The Z-stack images of nanofibers were recorded from top to bottom with a 2.5 μm slice thickness through a depth of ~ 45 μm.

2.2.16. Statistical Analysis

SEM results were presented as mean ± standard deviation. The interactions between different groups in cell culture were studied using analysis of variance (ANOVA) with a 95% confidence interval and Tukey's post hoc test. The results were expressed as mean ± standard error mean, and $p > 0.05$ were not considered significantly different, whereas values of $p < 0.05$ were considered significant. Data analysis was performed using Graph Pad Prism 6.5 software (Graph Pad, San Diego, CA, USA).

3.RESULTS

3.1. Physical Properties of Solutions

Major parameters such as working distance, applied voltage, and flow rate affect the results of the ES process. Changing these parameters causes alterations in the morphology and diameter of the produced fibers. Ambient conditions such as temperature and humidity also affect fiber formation. At the same time, the parameters such as surface tension, density, electrical conductivity, and viscosity may lead to a change in the morphology of the fabricated fibers.

The addition of D_3, K_2, and Mg at 10%, 1.25%, and 5% (w/w) concentrations, respectively, to the mixed solution of PLA(TCP)/PCL 1:1 (v/v), caused a decrease in the surface tension (Figure 1a). While the surface tension of pure PLA(TCP)/PCL solution was 27.6 ± 2.2 mN/m, it dropped to 27.1 ± 1.9 mN/m by adding APIs. A decrease in viscosity from 24510 to 22870 MPa s and in density from 1.327 to 1.318 g/ml were observed by adding APIs to the pure solution (Figure 1b

and 1c). Besides, an increase in electrical conductivity from 0.5 to 0.6 µS/cm was observed (Figure 1d). The physical parameters of the solutions are proper for the production of fibers. The fiber diameter of DKMF slightly increased compared to pure fiber. The reason for that may be a decrease in the viscosity of the APIs-added solution although there is an increase in its electrical conductivity.

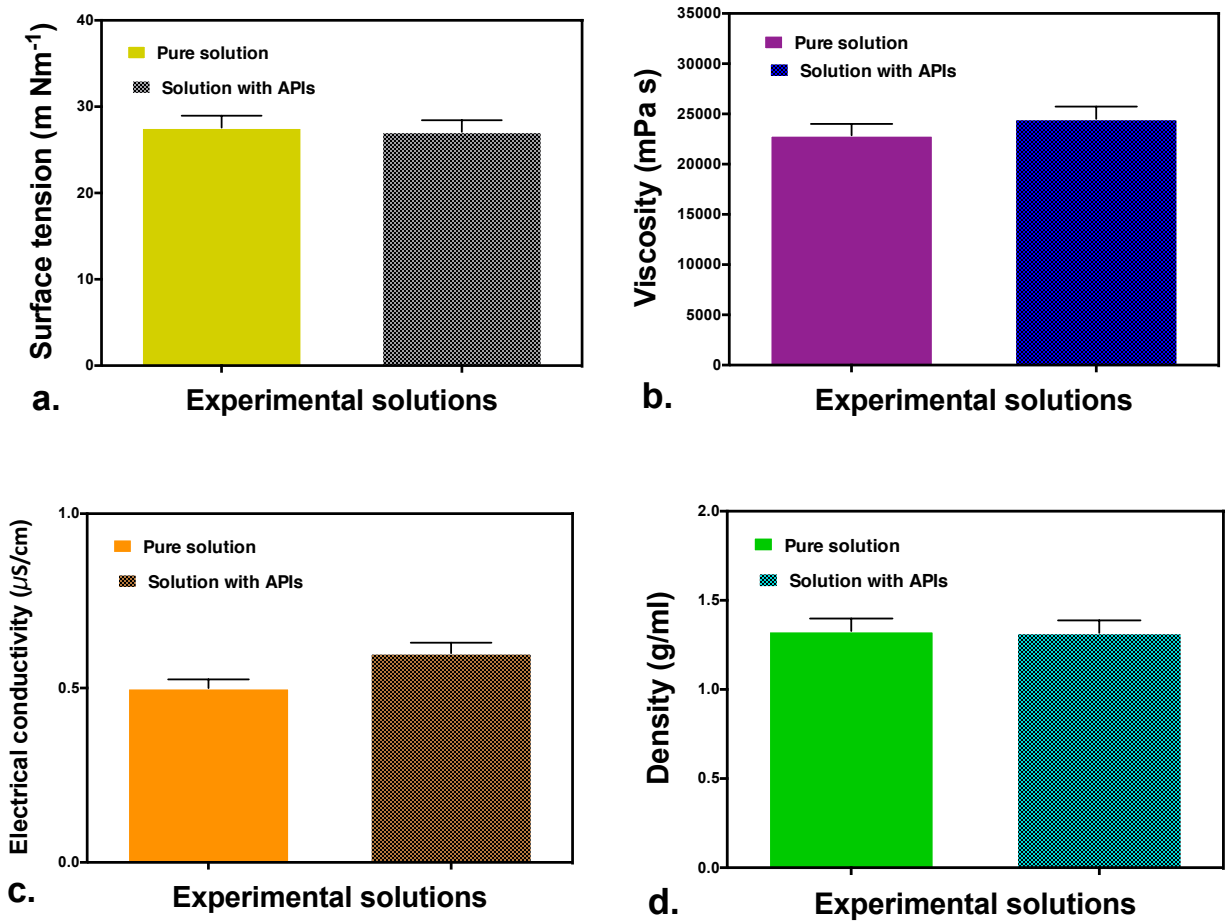

Figure 1. Physical parameters of solutions: (a) Surface tension, (b) viscosity, (c) electrical conductivity, and (d) density. APIs: Active pharmaceutical ingredients.

3.2. Morphological Characterization of Fibers

SEM was used to analyze changes in the morphology and diameter of nanofibers. All SEM images were given in Figure 2. PLA, TCP, and PCL polymers were used to produce fibers by ES. Firstly, PLA (12%, w/v) and TCP (5%, w/v) mixture were prepared in the same pot, and then this mixture was mixed with PCL (12%, w/v) solution at three different ratios, which are 1:3, 3:1, and 1:1 (v/v), for the production of fibers. According to the results obtained by SEM for

pure PLA(TCP)/PCL fibers, the optimized ratio was chosen as 1:1 (v/v) ratio due to its more homogeneous and smoother fiber surface. Hence, D_3, K_2, and Mg were loaded in this ratio. Also, the 1:1 (v/v) ratio was chosen to decrease the TCP ratio further because these fibers' production aims to strengthen the bone structure. The beads in the SEM image of PLA(TCP)/PCL (1:1, v/v) fibers originate from the structure of TCP and reflect its normal morphology.

The applied voltage to produce the fibers was 24 and 25 kV for all pure fibers and DKMF, respectively. The flow rate was tried between 0.08-0.38 ml/h. On the other hand, the working distance was fixed to 150 mm for all pure fibers while it was increased to 200 mm for DKMF.

The diameters of pure PLA(TCP)/PCL fibers at three different blend ratios are 1645.9 ± 364.8 nm, 1146.5 ± 197.9 nm, and 737.5 ± 126.3 nm for 3:1, 1:3, and 1:1 (v/v), respectively. The diameter of DKMF is 745.1 ± 131.7 nm. According to SEM results, the diameter of DKMF increased compared to pure PLA(TCP)/PCL(1:1, v/v) fibers (Figure 2d). At the same time, PLA(TCP)/PCL (3:1, v/v) fibers with a high TCP ratio were found to be too tough and nonhomogeneous (Figure 2a). PLA(TCP)/PCL (1:3, v/v) fibers were smooth but not homogeneous, and also, its average diameters were not in the nanoscale (Figure 2b). Fiber with the best morphology and fiber diameter was obtained at 1:1 (v/v) blend ratio for the PLA(TCP)/PCL (Figure 2c).

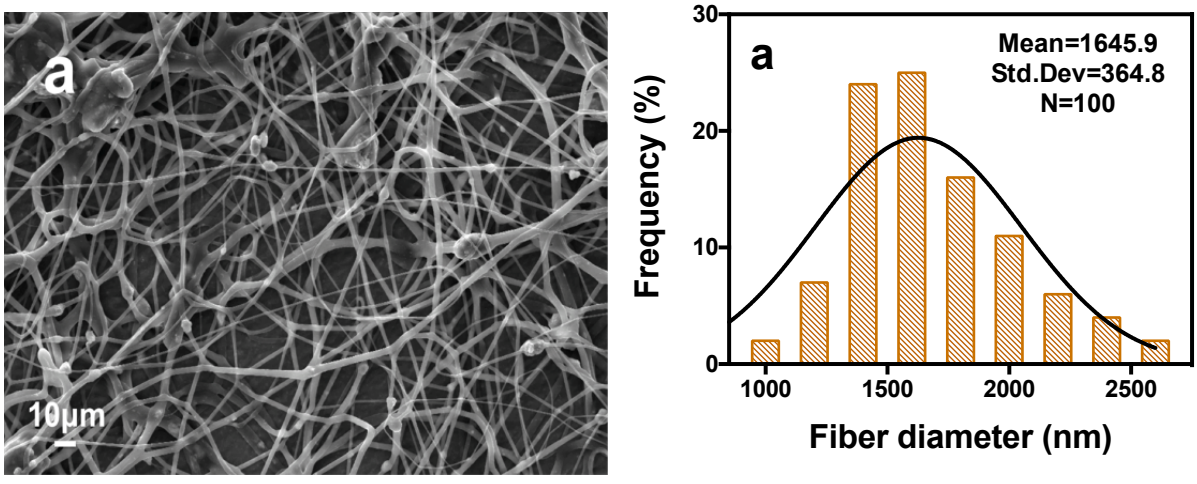
a
10μm
a
Mean=1645.9
Std.Dev=364.8
N=100
Frequency (%)
Fiber diameter (nm)

346

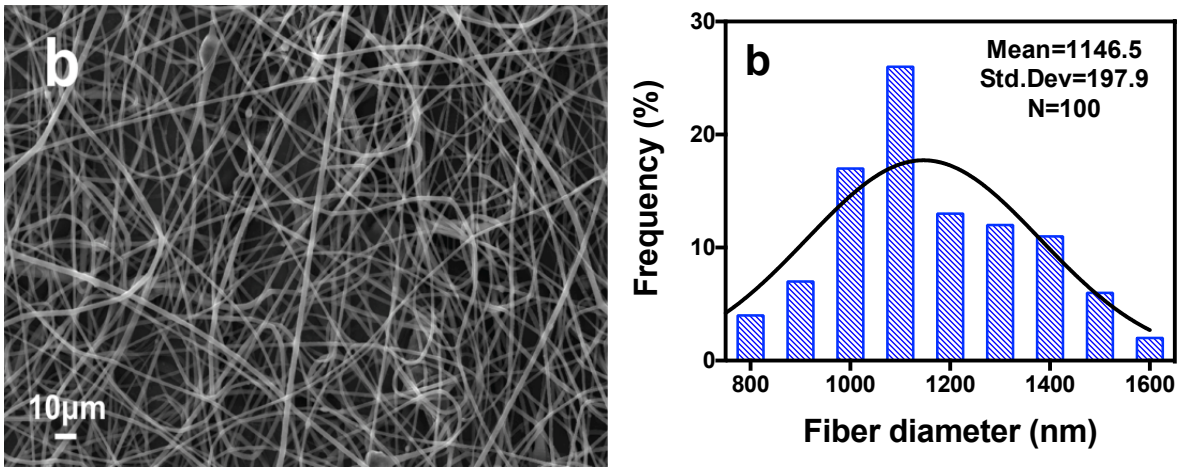
b
10μm
b
Mean=1146.5
Std.Dev=197.9
N=100
Frequency (%)
Fiber diameter (nm)

347

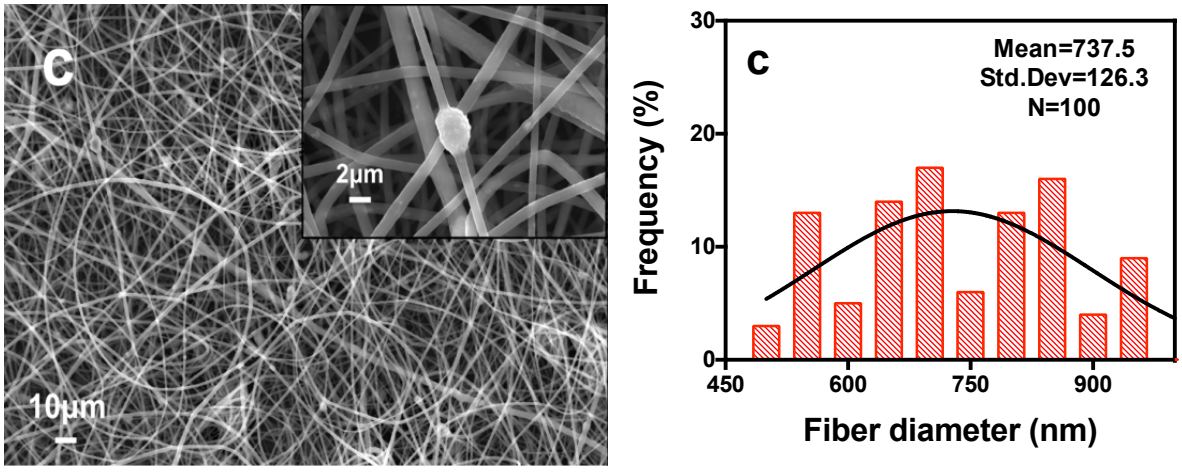
c
2μm
10μm
c
Mean=737.5
Std.Dev=126.3
N=100
Frequency (%)
Fiber diameter (nm)

348

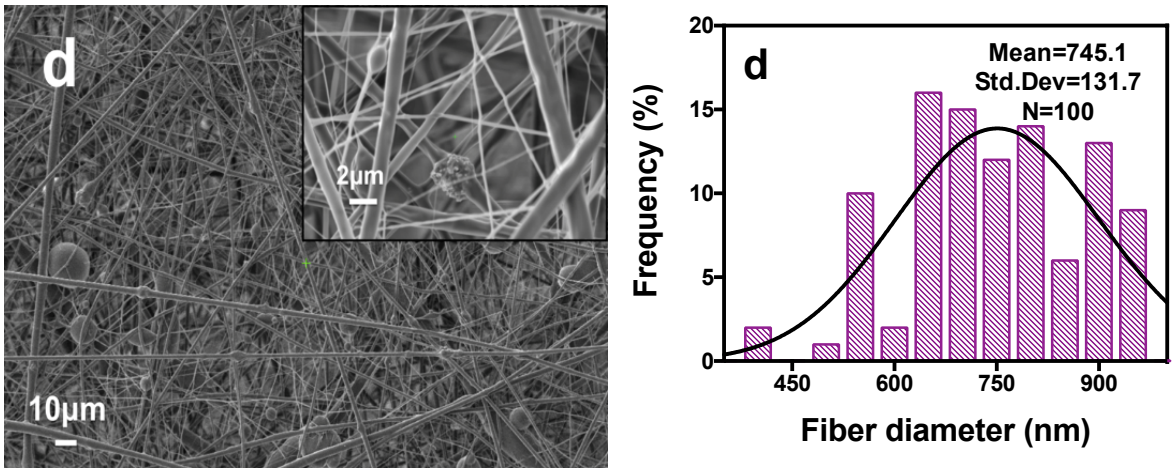

Figure 2. SEM images and fiber diameter distributions of DKMF and pure nanofibers: (a) PLA(TCP)/PCL (3:1, v/v) fiber, (b) PLA(TCP)/PCL (1:3, v/v) fiber, (c) PLA/TCP/PCL (1:1, v/v) fiber, and (d) DKMF (1:1, v/v) fiber. N = 100 in all diameter distributions.

3.3. Fourier-Transform Infrared Spectroscopy (FTIR)

Figure 3a showed the FTIR spectra of nanofibers with different compositions to characterize functional groups, verify the existence of the components in fibers, and discriminate prospective chemical changes between phases. The characteristic peaks at 2940.9 cm^{-1}, 2865.7 cm^{-1}, 1722.2 cm^{-1}, 1293.0 cm^{-1}, 1238.0 cm^{-1}, and 1168.0 cm^{-1} belong to PCL. These peaks characterize asymmetric CH_2 stretching, symmetrical CH_2 stretching, C=O stretching vibration, C-C and C-O stretching vibration, asymmetrical C-O-C- stretching vibration, and C=O-C stretching vibration, respectively.[27] In the PLA spectrum, some specific peaks represent C=O ester carbonyl groups at 1747.2 cm^{-1}, C-H deformation at 1453.1 cm^{-1} and 1360.5 cm^{-1}, C-O stretching at 1181.2 cm^{-1} and 1082.8 cm^{-1}, and C-C stretching at 866.9 cm^{-1}.[28] PCL and PLA are aliphatic polymers with an analogous structure. Peaks at 962.3-1022.1 cm^{-1} and 559.3-599.8 cm^{-1} are specific for TCP. These represent the stretching mode and vibration peaks of the PO_4^{3-} in TCP, respectively.[29] In Mg spectrum, peaks at 2916 cm^{-1} and 2854 cm^{-1} are associated with C-H stretching. On the other hand, the peak at 1464 cm^{-1} belongs to symmetrical carboxylate (COO-) stretching vibration.[30] In the D_3 spectrum, a peak at 3232.1 cm^{-1} is associated with the O-H bond, and the peak at 1640 cm^{-1} belongs to H-C=C-H stretching vibration.[31] The peak at 991.2

cm^{-1} belongs to vitamin K_2 and characterizes the -C-C- strain vibration. These results prove that PLA, PCL, TCP, Mg, D_3, and K_2 were successfully loaded in composite nanofiber.

3.4. X-ray Powder Diffraction (XRD)

XRD is a rapid and nondestructive analytical method used to examine the structure and crystalline forms of the nanofibers.[32] Figure 3b-i gives the XRD results of the samples. Looking at the XRD result of PLA, two diffraction peaks were detected at 2θ = 16.4° and 22.6°.[33] PLA was less pronounced than PCL due to its lower crystal absorption density and showed a more pronounced amorphous scattering. This situation may be due to different degrees of molecular deformation during the ES process. Two sharp crystalline peaks with a high degree of crystallinity and strong absorption density at 2θ = 21.4° and 23.8° have belonged to PCL.[34] Very sharp peaks at 2θ = 11.2-29.5° range in the XRD results of pure TCP have been observed. Although not as sharp as the others, there were also peaks in the range 2θ = 31.4-60.0°, which proved that TCP has a crystal structure.[35] According to XRD results, Mg was found to have a high crystal structure, and sharp peaks were detected at 2θ = 18.5°, 26.2°, 35.1°, 44.1°, 55.0°, and 58.04°. Very sharp peaks at the 2θ = 10.2-27.5° range of pure D_3 have been observed in the XRD results. There were also peaks in the range 2θ = 30.5-55.2°. These peaks are characteristic of D_3 and prove that D_3 has a highly crystalline structure. In the XRD results of pure K_2, sharp peaks were observed at 2θ = 44.1°, 64.4°, and 77.5°. At the same time, a prominent and wide peak was observed between 2θ = 18.0-20.0°. This peak is characteristic for K_2 show that it has a crystalline structure. All polymer peaks, which belong to PLA, TCP, and PCL observed by five distinct peaks and wide amorphous scattering, were seen in the XRD results of pure nanofiber. However, four of these peaks had low absorption density. The structure of DKMF was found more crystalline compared with pure nanofiber. The reason is that Mg, K_2, and D_3 in DKMF have crystalline structures. The peaks belong to APIs were observed in the XRD line of DKMF. Therefore, it can be said that the APIs were successfully loaded in DKMF.

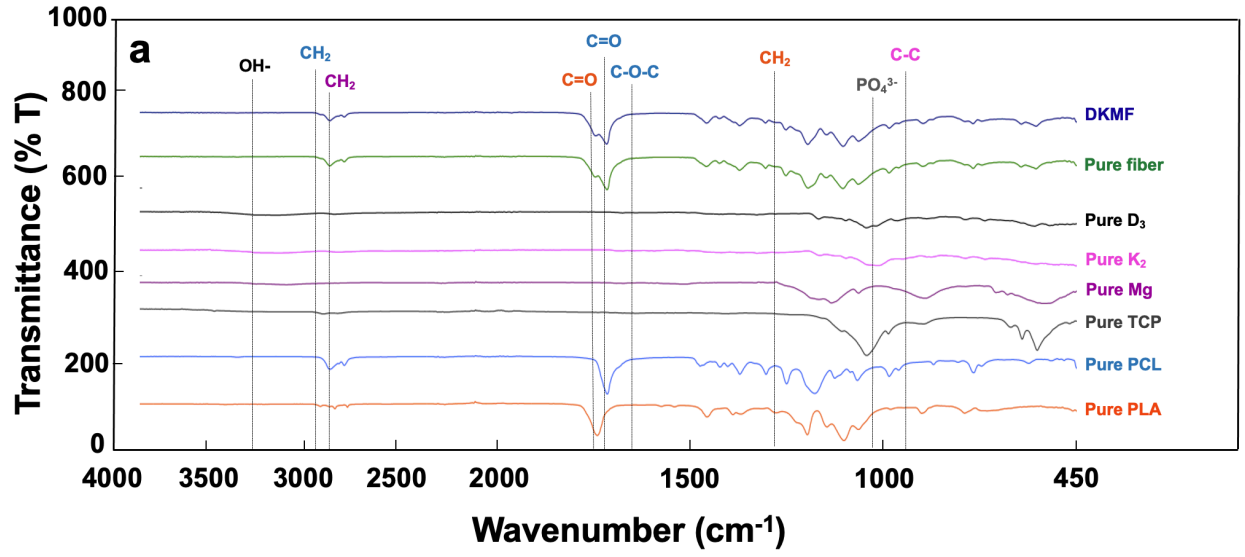

394

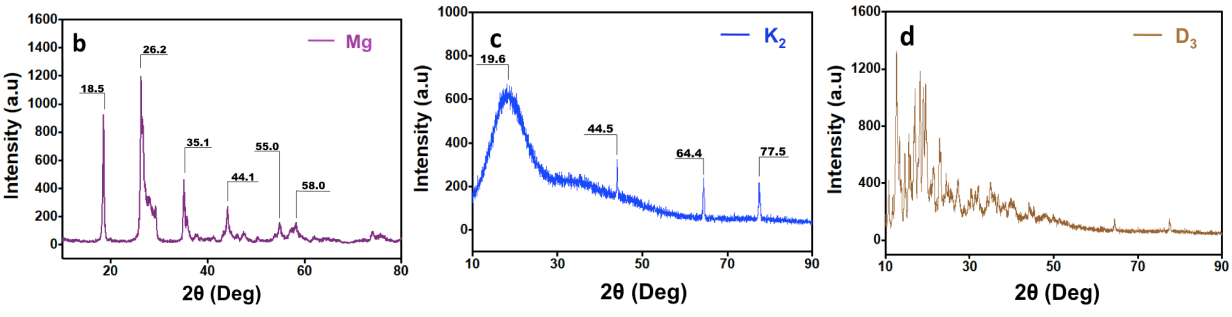

395

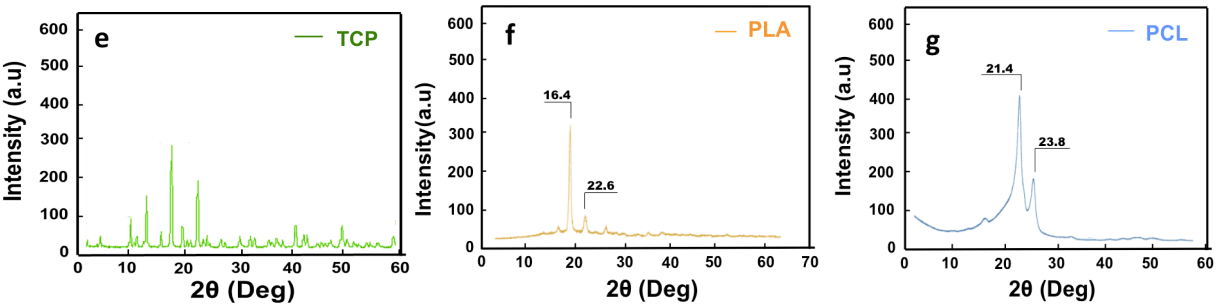

396

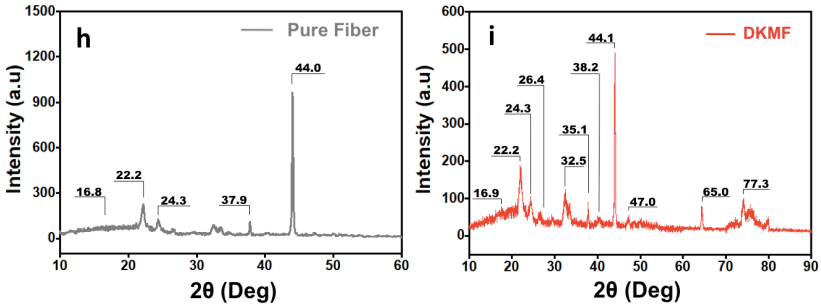

397

398 **Figure 3.** (a) FTIR spectrums of pure PLA, PCL, TCP, Mg, K_2, D_3, pure nanofiber, and DKMF.

399 XRD results of pure (b) Mg, (c) K_2, (d) D_3, (e) TCP, (f) PLA, (g) PCL, (h) pure fiber, and (i)

400 DKMF.

401

3.5. Tensile Test of Fibers

A tensile test was used to characterize the mechanical and tensile properties of nanofibers. Figure 4 showed the effects of D_3, K_2, and Mg on the tensile strength and strain at break of fibers. It was determined that the tensile strength of DKMF was higher than pure fibers. The tensile strength of pure fibers and DKMF were 30.4 ± 10.2 and 70.8 ± 24.2 kPa, respectively. According to the tensile test results, an increase in the mechanical strength of DKMF was obtained after loading of D_3, K_2, and Mg in fiber (Figure 4a).

On the other hand, the strain at break of pure fibers was higher than DKMF (Figure 4b). It is seen from the stress-strain curve, and both samples have a hard and tough structure. On the other hand, loading drugs to fiber made them tougher but less flexible. Because at the beginning of the curves (zoomed in Figure 4c), DKMF samples gave steeper and sharper peaks compared to pure fiber samples. The reason for that D_3, K_2, and Mg have crystalline structures. Thus, they have higher strength but lower structural flexibility for interaction with adsorbate molecules due to their crystalline structures. [36]

3.6. Differential scanning calorimetry (DSC)

DSC results were given in Figure 4d-e. In the DSC analysis between 0-200°C temperatures, the melting (Tm) and glass transition temperature (Tg) of fibers were examined. When comparing the DSC results of DKMF with pure fiber, a slight decrease in Tm and Tg values was observed for DKMF. The Tg value of pure nanofibers and DKMF was 63.2°C and 60.9°C, respectively. On the other hand, the Tm values of pure nanofibers and DKMF were 154.4°C and 151.5°C, respectively. Looking at the changes in values, it is clear that there is no significant change in the operating temperature range between Tg and Tm for DKMF and pure nanofibers. According to the results, loading D_3, K_2, and Mg to fibers caused a slight change in the thermal behavior of the fiber.

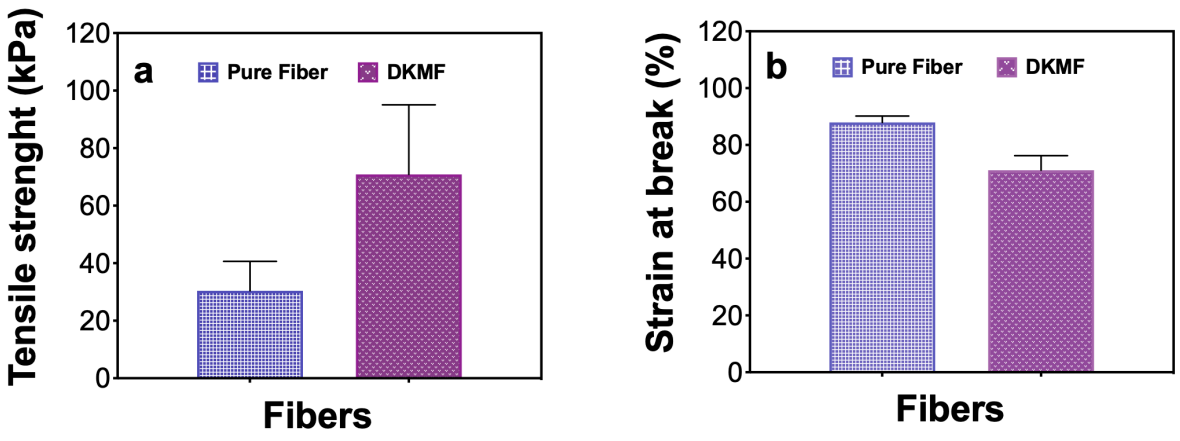

426

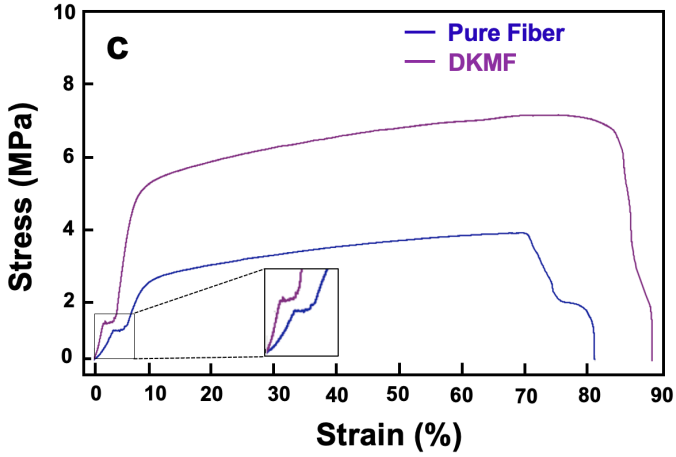

427

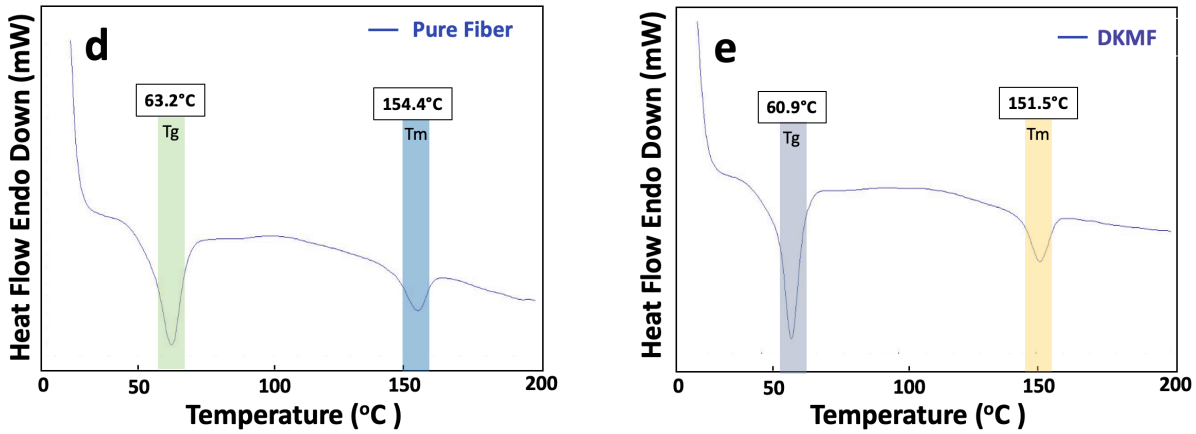

428

429 **Figure 4.** Tensile properties of nanofibers: (a) Tensile strength, (b) strain at break, and (c) tensile
430 stress-strain curves. DSC results of nanofibers: (d) Pure fiber and (e) DKMF.

431 **3.7. *In Vitro* Drug Release Test**

432 *In vitro* drug release test was carried out to investigate the releasing behaviors of D_3, K_2, and Mg
433 released from DKMF for 144 h. PBS (pH 7.4, 37°C) was used to mimic the physiological
434 conditions of living organisms during the drug release test process (Figure 5). In the beginning,

435 UV spectroscopy was used to construct the linear standard calibration curves of D_3, K_2, and Mg
436 (Figure 5d-f). Afterwards, EE was measured to evaluate whether APIs are loading to fibers
437 successfully or not, and EE was found 82.8%, 89.5%, and 81.3% for D_3, Mg, and K_2,
438 respectively (Figure 5j).
439 D_3 was released in a burst release manner at the end of the 3rd and 5th day by releasing its 29.7%
440 and 30.0%, respectively, but it demonstrated sustained release by 81.7% during the rest of the
441 test period (Figure 5g). On the other hand, Mg among all ingredients was released in a sustained
442 release manner in the first 72 h by releasing its 59.0% from DKMF. However, it showed a burst
443 release profile by releasing its 40.8% in 24 h, and then, a sustained release was exhibited for the
444 remaining of Mg during the rest of the test period (Figure 5h). The release behavior of K2 was
445 more sustainable than the other two APIs and it was released lesser than the other two APIs by
446 releasing 69.0% in 144h (Figure 5i).

447 **3.8. *In Vitro* Drug Release Kinetics**

448 To analyze the release kinetics of Mg, D_3, and K_2 from DKMF that were incubated in dynamic
449 conditions in PBS (pH 7.4, 37^{o}C), the Hixson-Crowell, zero-order, and first-order release models
450 were used in this study. Mg, D_3, and K_2 with higher R^2 values were released from DKMF
451 according to the zero-order, zero-order, and Hixson-Crowell model, respectively (Table 1 and
452 Figure 6).

453 **Table 1.** Results of mathematical drug release models for all nanofibers. D_3: D_3 vitamin released
454 from DKMF. Mg: Mg released from DKMF. K_2: K_2 vitamin released from DKMF.

	Zero-Order		**First-Order**		**Hixson-Crowell**	
Sample	R^2	K_0	R^2	K_1	R^2	K_{hc}
D_3	0.9207	0.4483	0.8188	-0.0036	0.8637	0.0103
Mg	0.9440	0.7357	0.8981	-0.0265	0.9306	0.0328
K_2	0.9717	0.4539	0.9796	-0.0033	0.9799	0.0098

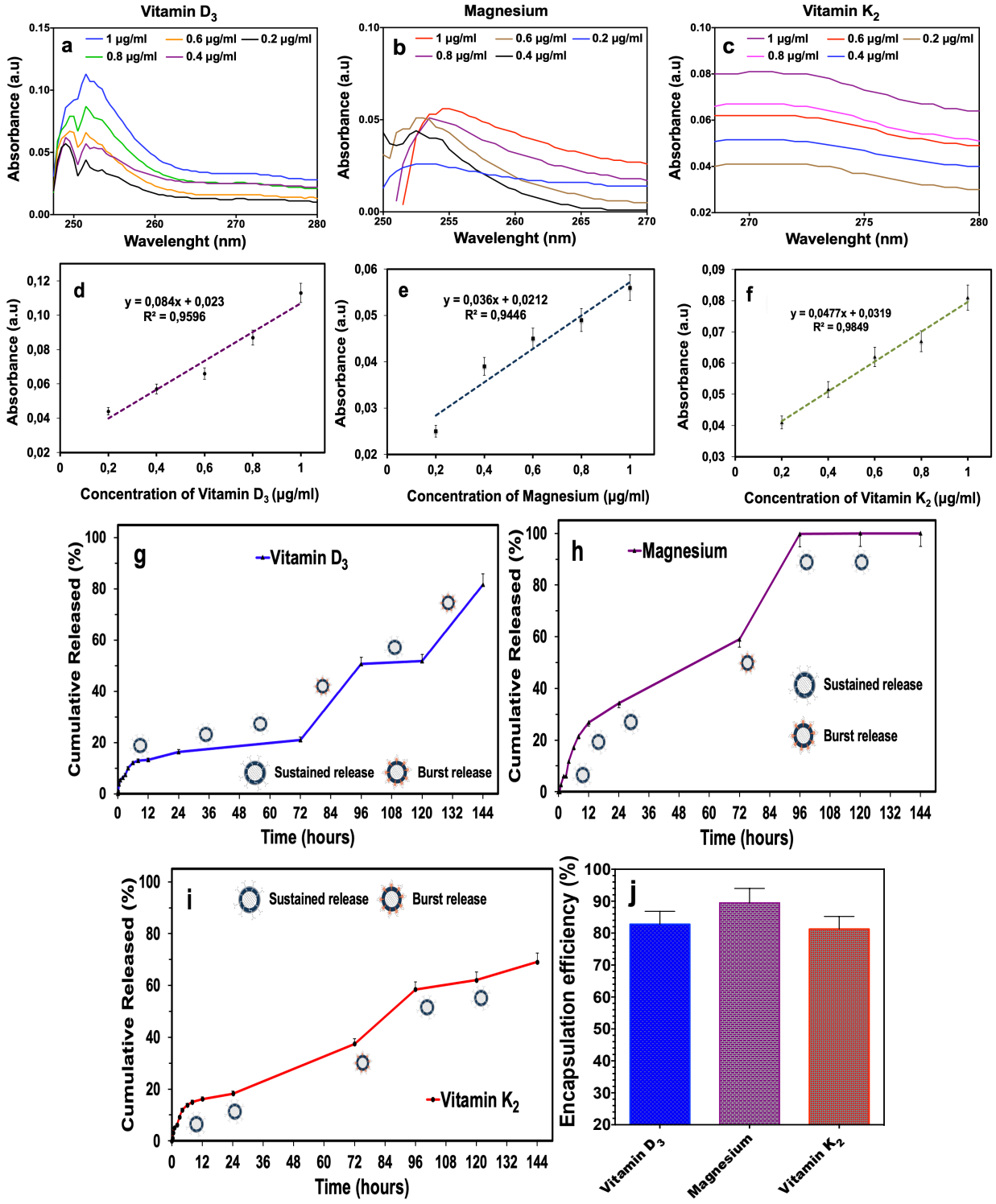

Figure 5. *In vitro* drug release profiles of fibers: Absorption spectra of (a) D_3, (b) Mg, (c) K_2, calibration curves for (d) D_3, (e) Mg, (f) K_2, release profiles from the DKMF for (g) D_3, (h) Mg, (i) K_2, and (j) encapsulation efficiency for D_3, Mg, and K_2. All the measurements were repeated three times, and the errors were less than 5%.

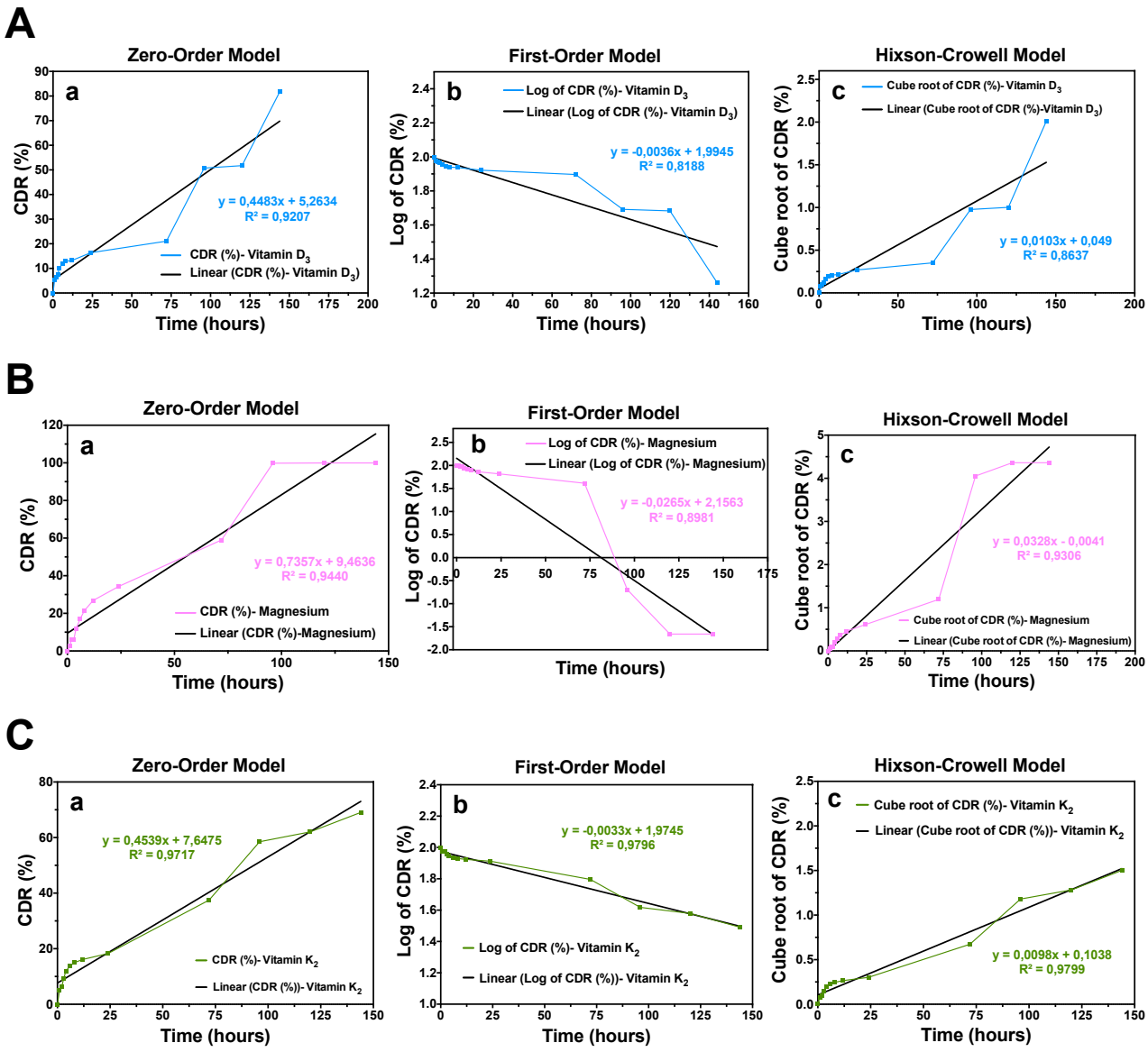

Figure 6. The release kinetic models of D_3 (A), Mg (B), and K_2 (C) release profiles from the DKMF: (a) zero-order, (b) first-order, and (c) Hixson-Crowell models.

3.9. *In Vitro* Degradation Test

The healing of the bone defect typically is completed within 40 days, but sometimes it could be take up to 6 months depending on changing conditions and size of the defect. Therefore, a material used to treat bone defect should remain functional for at least 40 days.[37] It is why the degradation properties of DKMF and pure fibers were evaluated throughout 41 days in this study. On the other hand, PLA, PCL, and TCP are applied as bone substitute materials at implantation sites due to their biodegradable properties. Besides, reduced local pH, induced inflammatory reactions, and accelerated degradation are observed after the degradation of PLA.

Therefore, PCL is added to reduce the inflammatory response and minimize local acidification. In addition to these effects, TCP also improves the osteoconductivity and bioactivity properties of nanofibers.[37, 38] The degradation of structures generally accelerates after adding the APIs. In this study, 35.3% of pure nanofibers and 26.4% of DKMF degraded at the end of 41 days. Even if the healing of the bone defect takes 6 months, it is estimated that DKMF will remain effective in the treatment according to its degradation rates. The crystalline structures of APIs cause the reason in the decrease on degradation ratio of DKMF.[39] The mass loss evaluation of nanofibers during their degradation process was shown in Figure 7a.

3.10. *In Vitro* Swelling Test

The swelling ratio of nanofibers is affected by many different physical parameters such as polymer concentration, pH, surface area, cross-linking, and porosity. In addition to these parameters, there is a relationship between the diameter and swelling ratio of nanofibers.[40, 41] The water up-take capacity enhances with the increase of fiber diameter.[42] In this study, the swelling ratios of DKMF and pure nanofibers were measured as 371.6% and 329.6%, respectively. In addition, a direct proportion was observed between swelling ratio and tensile strength of nanofibers. The water up-take capacity increases, and degradation decreases with the enhancement of nanofiber strength (Figure 7b).[43]

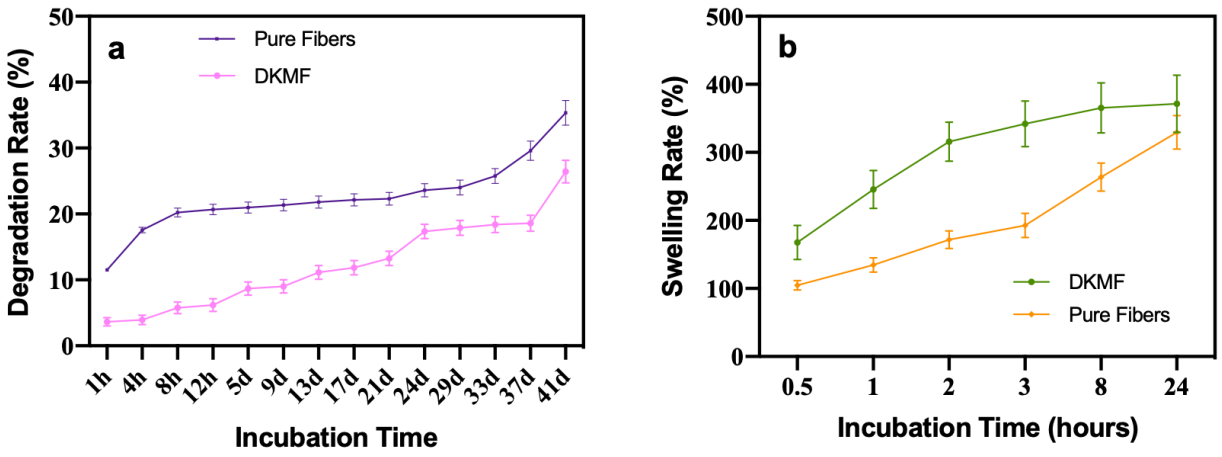

Figure 7. *In vitro* degradation test (a) and swelling behavior (b) of pure nanofibers and DKMF. The tests performed by taking three samples from each nanofiber represent the mean ± standard error of the mean.

3.11. Cytotoxicity of Nanofibers

The effect of pure nanofibers and DKMF on fibroblast cell viability was determined after 24 h using the WST assay. The results showed no significant decrease in viable cell number. Compared to the control group, in which the cells were cultures in the medium without nanofibers, the cells cultured with pure nanofibers and DKMF showed 89.5% ± 7.4 (p=0.2995) and 78.7% ± 6.9 (p=0.0890) viability, respectively (Figure 11). There is no significant difference in the viability of cells between DKMF and pure nanofibers (p=0.506). The apoptotic or necrotic cells were not observed during the culture. The nanofibers restricted the proliferation of cells rather than the cytotoxic effect (Figure 8a).

3.12. Differentiation Into Osteogenic Cell Lines

Under normal culture condition with pure nanofibres, any change in the expression of osteogenic differentiation markers (Runx2, osteopontin, and BMP2), the chondrogenic differentiation marker (Sox9), and the adipogenic differentiation marker (PPAR-γ) were not observed compared to the control culture without the nanofibers (Figure 8b).

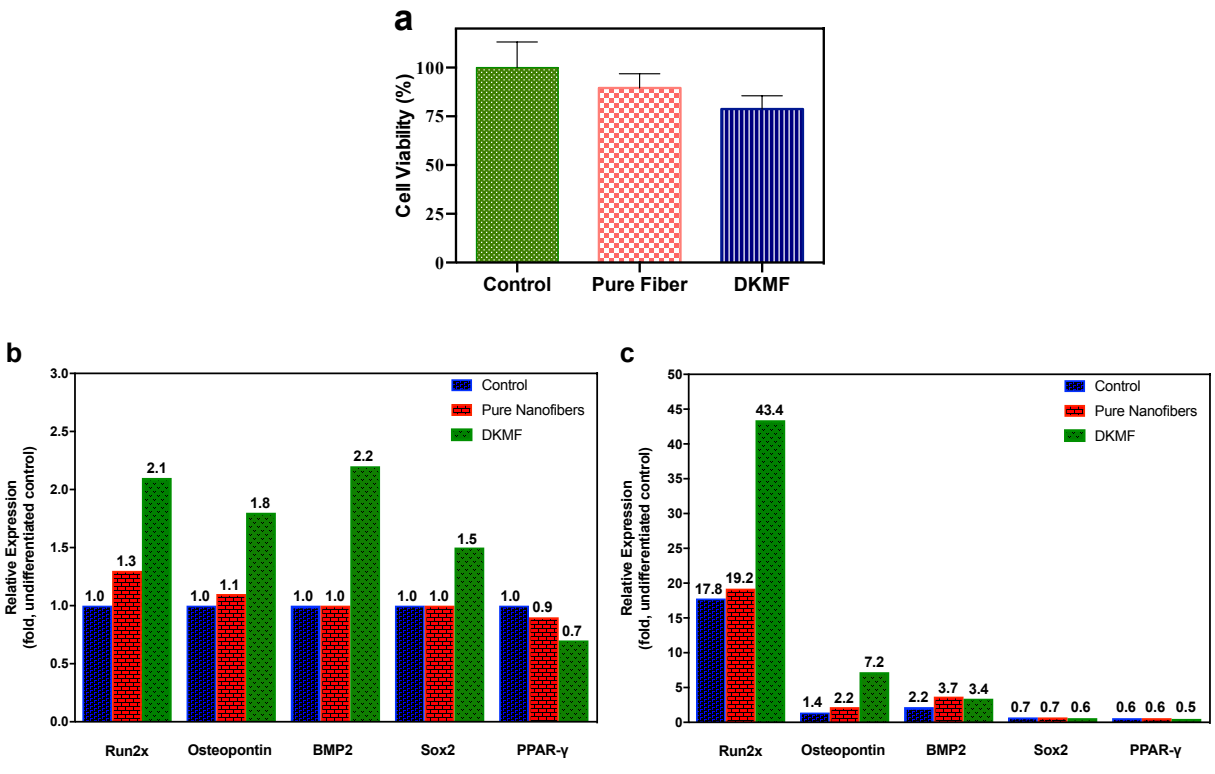

Figure 8. (a) Viability of fibroblasts after the culture with DKMF and pure nanofibers in DMEM. The cell viabilities were expressed in percentage with respect to the control culture, in which fibroblasts were cultures in the same medium without any nanofibers. The gene expression analysis of hBM-MSCs before (b) and after (c) the culture in the osteogenic differentiation medium for two weeks. The effects of pure nanofibers and DKMF were compared with the cells incubated without nanofibers (control). The expression levels were presented as fold-expression with respect to the control group. ActB was used as a housekeeping gene.

In the culture with DKMF, the expression of osteogenic markers was induced slightly under the effect of D_3, K_2, and Mg. In these cultures, the medium was not supplemented with the chemical cocktail to differentiate the cells, but APIs-loaded nanofibers induced cell differentiation. Almost a 2-fold increment in the expression of Runx2, osteopontin, and BMP2 was observed (Figure 8b).

Nanofibers demonstrated a significant effect in the differentiation medium, in which the supplements were provided for the cells to differentiate into osteogenic cells. After two weeks of differentiation, the cells expressed Runx2 that is the early osteogenic differentiation marker. Although this marker was also expressed by the control cells in the differentiation medium at 17.8-fold compared to the undifferentiated control cells, the expression was 19.2-fold in the culture with pure nanofibers and 43.4-fold in the culture with DKMF (Figure 8c). When compared the Runx2 expressions of DKMF to the undifferentiated control cells, the differentiation efficiency of stem cells was improved about 21-fold under the effects of D_3, K_2, and Mg. On the other hand, the Runx2 expression was improved by 2.44-fold compared to the cells in the differentiation medium without fibers. To observe the impact of nanofibers on the chondrogenic and adipogenic differentiation, the expression of Sox9 and PPAR-γ were analyzed. While the osteogenic markers were highly expressed during the differentiation, the expression of

Sox9 and PPAR-γ was suppressed compared to the control simultaneously, and the inductive effect of DKMF could not be observed (Figure 8c).

3.13. Cell morphology

On days 1, 3, and 7, after seeding osteoblast cells in nanofibers, the disseminated cells attached to the surface of nanofibers were clearly shown in the SEM images (Figure 9). The osteoblast cells were seeded on nanofiber that provides cells with a larger 3D surface area for growth. The nanofiber pores allowed fluid and cells to seep into nanofibers. DKMF can clearly show that cells are spreading and proliferating on the surface. Also, after 7 days of incubation, DKMF was found to promote large axonal sprouting and needle-like elongation of osteoblast cells.

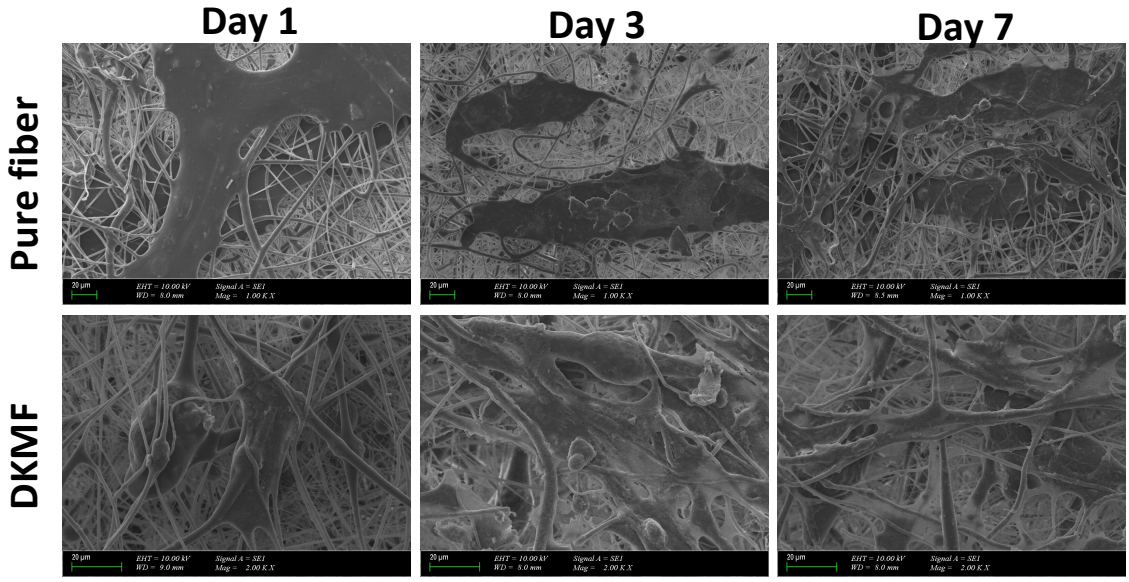

Figure 9. SEM images of attachment of osteoblast cells into scaffolds after incubation period on days 1, 3, and 7.

Osteoblast cell morphologies were also confirmed using confocal laser scanning microscopy. The nuclei and cytoskeletons of cells on nanofibers were stained with DAPI and F-actin, respectively. As shown by the confocal images (Figure 10a), on days 1, 3, and 7 of incubation, rounded nuclei with a cytoskeleton were noticeably observed in DKMF. When the incubation time could be extended to 7 days, DKMF promoted cellular attachment, improving the cytoskeleton and cell-cell interaction.

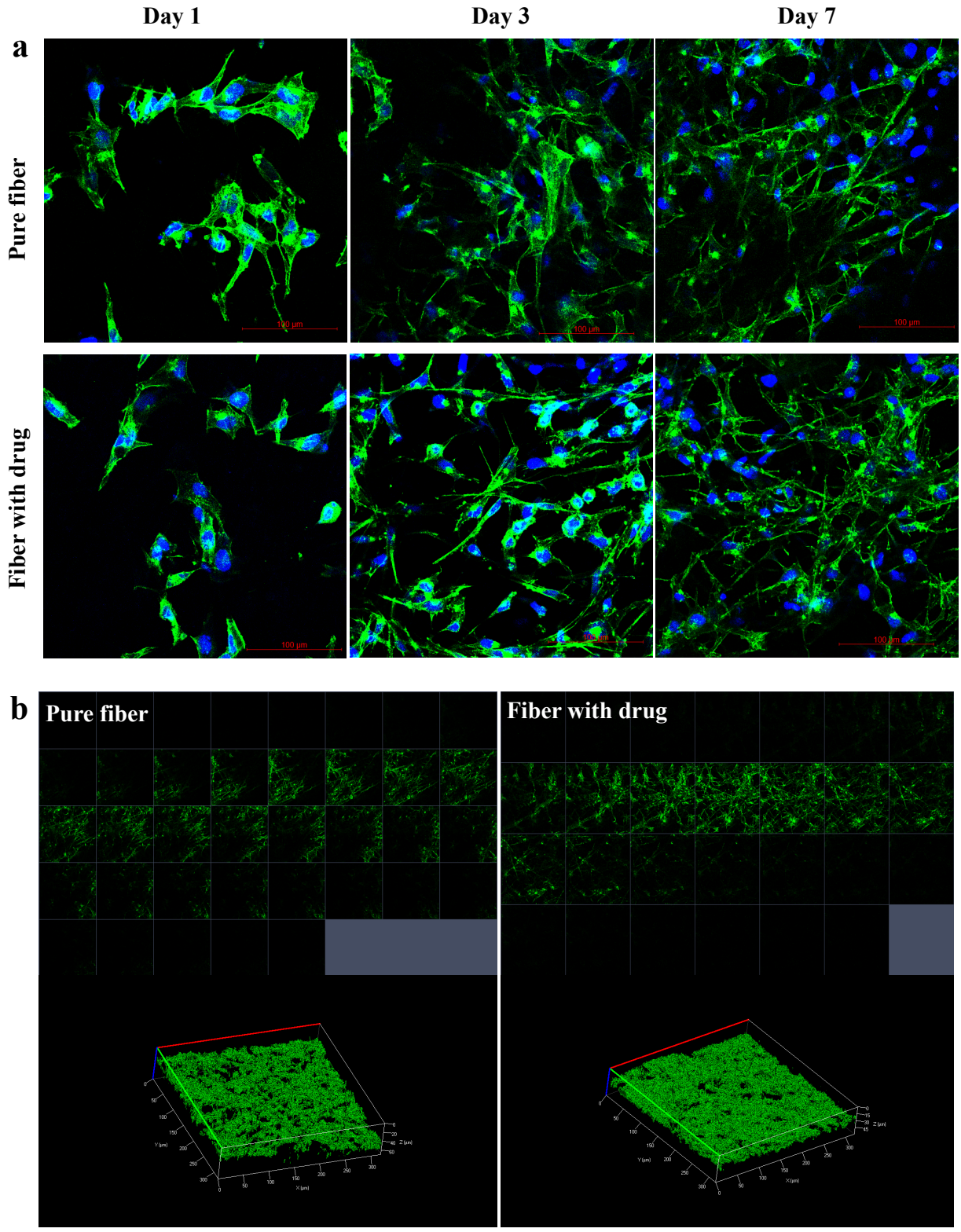

Figure 10. Confocal microscopy images of osteoblast cells seeded on nanofibers. Cells on nanofibers were stained with DAPI to display blue (nuclei) and F-actin to display a green (cytoskeleton). The Z-stack images of optical confocal images from top to bottom with a 2.5 µm slice thickness and the reconstructed 3D projection image of cells on scaffolds after incubation period on day 7.

Figure 10b showed Z-stack images of top surface-to-bottom optical slices in nanofibers with a slice thickness of 2.5 μm and 3D reconstructions of cells within nanofiber. Optical slicing of the sample in the Z-direction, as shown in Figure 10b, allowed us to monitor the penetration of cells into the scaffolds after 7 days of incubation. It was observed that cells infiltrated the nanofibers at a depth of 45 μm from the upper surface of nanofibers. These results demonstrate the successful growth, proliferation, and infiltration of cells within nanofibers, indicating their suitability for bone tissue applications.

4. DISCUSSION

The damage and degeneration are observed in bone tissues because of injuries, diseases, and trauma. Treatment of damaged and degenerated tissues is necessary to enable their regeneration and repairment. Bone tissue engineering is an encouraging field for the repair of bone. Techniques belonging to bone tissue engineering based on autogenous tissue transplantation are expected to solve supply limitation, immune rejection, and donor scarcity, which are limitations of autograft and allograft methods. On the other hand, this area is focused on using electrospun composite nanofibers and APIs-loaded nanofibers in the generation of bone structures. Therefore, bone tissue engineering has become a rapidly expanding area of research.[44]

Choosing the suitable material in tissue engineering applications depends on several properties such as biocompatibility, toxicity, and the immune response by the body.[45] In previous bone tissue engineering studies about bone regeneration, it has been found that PLA, TCP, and PCL were used singly or in binary combination to produce electrospun composite fibers.[10, 46] In our study, FDA-approved PCL and PLA were chosen as the carrier system and scaffold for bones due to their biodegradability and mechanical properties.[8, 47] Also, the FDA-approved TCP, a porous ceramic, was chosen because it provides strength to the bones.[48] The primary function of D_3 is to maintain concentrations of serum phosphorus and calcium, hence, essential cellular functions were protected and mineralization of the skeleton was encouraged.[13] On the

other hand, K_2 is essential for calcium usage and inhibits arterial calcification, and strengthens the bones. [16] Mg is an intracellular cation that helps to bone stabilization, bone growth, and mineralization. [18] Thus, these three polymers and three active ingredients were used to produce DKMF as a fiber composite, and this is novel.

According to the SEM results of pure fibers, beads were observed in all images of fibers produced. McCullen et al. reported that the addition of TCP causes an origination of beads in the fibers.[49] Therefore, in this study, PLA(TCP)/PCL at 1:1 (v/v) concentration was selected as the optimized ratio for nanofibers due to its nanoscale diameter and better morphology compared to other ratios. After that, D_3, K_2, and Mg were loaded to the fibers in the optimized composite ratio. Then, the characteristic bands and molecular structure of APIs and polymers were observed in the fibers by performing XRD and FTIR tests. Thus, obtained results proved that Mg, D_3, K_2, PLA, PCL, and TCP were successfully loaded in nanofibers.

In bone tissue engineering, it is accepted that fibers have mechanical strength as close as possible to the strength of the bone to be repaired, although there are no precisely defined criteria for the mechanical properties of fibers. Bones have a balanced mixture of tough and soft materials. A primary component of bone is collagen, which composes a soft protein for the calcium phosphate that provides bone with its hardness and strength. The mixture of tough and soft materials enables bone to be flexible enough to withstand impacts but rigid enough to support its structural integrity.[50] According to the tensile test results, pure fiber was proper for bone tissue engineering with its hard and tough structure, but loading APIs to fibers made the structure of nanofibers more proper by making it softer. On the other hand, a slight decrease in Tm and Tg values was observed after loading APIs to fibers. The reason for this decrease may be due to the structural differences and interactions between polymers and APIs.[51] Furthermore, the water up-take capacity was found to increase with fiber diameter and strength.[42] However, the decrease in the degradation ratio depends on the correlation between diameter and strength.[52]

614 EE is the percentage of the drug, which is successfully loaded in the fibers. Mg was determined
615 as the API having the highest EE due to its high solubility in PBS. EE was lower for D_3 and K_2
616 than Mg due to their low solubility in PBS, although Tween 80 was added to PBS to increase the
617 solubility of D_3 and K_2.[53] The drug-to-polymer ratio or low concentration of emulsifier may be
618 another reason that influences the drug loading.[24]
619 The drug release analysis was performed to investigate the release kinetics of drugs encapsulated
620 in the fibers for 144 h with PBS that mimics the physical conditions of living organisms. All of
621 the D_3, K_2, and Mg exhibited sustained release for 72 hours. The D_3 was released in a burst
622 manner between 72-96 h and 120-144 h. K_2 was released in a controlled manner within 144 h
623 except between 72-96 h. Mg was also released in a burst manner between 72-96 h. However, it
624 was released in a sustained release manner except for this time range. In this study, the D3, K2,
625 and Mg releases were observed for 144 hours by 81.7%, 69.0%, and 99.9%, respectively, in
626 DKMF. In the study, the burst release was limited and followed by a sustained release for 144 h,
627 similar to previous studies.[54]
628 The fibers well maintained the cell viability during the culture. The cell viability was slightly
629 reduced, but this reduction was still within the accepted limit for viable cells according to UNI
630 EN ISO 10993-5.[55] The cell growth was decreased without any significant loss of cell viability
631 during the stem cell differentiation.
632 In the typical cell culture, the cells were treated only with fibers and any induction for the
633 differentiation was directed by these fibers. Wnt signaling pathway was known to play a central
634 role in both cell proliferation and differentiation in mesenchymal stem cells.[56, 57] Previously,
635 it was demonstrated that the proliferation of bone marrow-derived mesenchymal stem cells was
636 induced under the effect of Wnt3a while suppressing the osteogenic differentiation in the
637 absence of BMP signaling.[58] DKMF increased the expression of BMP2 by almost 2-fold
638 accompanying the induction of Runx2 and osteopontin even in the absence of differentiation
639 medium. The cell differentiation might be the reason for the restricted cell growth under the

effect of fibers. Notably, the differentiated cell morphology could not be observed in the culture with DKMF without the differentiation medium. In the group with pure fibers, the cell proliferation was also slowed down. Therefore, the induction of differentiation could not be the only reason for restricted cell proliferation. Another reason might be the lack of a suitable surface for cell adhesion, which might limit cell proliferation.

Upon the induction of endogenously secreted BMP2 in the cells in response to DKMF, the expression of early osteogenic marker Runx2 was increased in the typical culture of our study. A similar observation was reported that the expression of osteogenic markers might be induced in response to Wnt3a with further increases in osteogenic differentiation markers after the BMP2 addition.[58] However, the differentiation could not be observed under sole canonical Wnt signaling without the BMP signaling, as it was observed in the normal cell cultures with pure fibers in our study.

In the early study on mesenchymal stem cell differentiation, it was proposed that the selective differentiation into either osteoblasts or chondrocytes might be controlled by manipulating the canonical Wnt signaling.[59] BMPs support both chondrocyte and osteoblast differentiation of mesenchymal stem cells, but the canonical Wnt signaling pathway exerts opposite activities to control the differentiation of osteoblasts chondrocytes. The canonical Wnt signaling suppresses chondrocyte differentiation by inhibiting Sox9 expression. During the early stage of osteoblast differentiation, Wnt signaling inhibits Sox9 expression while promoting Runx2 expression. As a result, the osteogenic differentiation progresses in the mesenchymal stem cells, but not the chondrocyte differentiation.

Vitamin D_3 and Vitamin K_2 were previously shown to support the differentiation of mesenchymal stem cells into osteogenic cells and bone tissue calcification.[17, 60] The expression of PPAR-γ inhibits the osteogenesis of mesenchymal stem cells by down-regulating the Wnt signaling and Runx2.[61] During the differentiation, the expression of PPAR-γ was decreased under the effect of DKMF. The chemical cocktail used for differentiation seems to

lead to this PPAR-γ-suppression, but a weak suppressive effect of DKMF on the PPAR-γ-expression could also be observed in the normal culture medium. In addition to its suppressive effect on the PPAR-γ-expression, DKMF induced the expression of Runx2, BMP2, and osteopontin in the early stage osteogenic differentiation. Both vitamin D_3 and vitamin K_2 were demonstrated to support osteogenesis, but the role of Mg is curious. The role of the kinase and cation channel TRPM7 and the magnesium transporter MagT1 in the osteogenic differentiation showed the importance of the magnesium ion in osteogenesis.[62] In this point, above a certain value of Mg concentration has an inhibitory effect on the osteogenic differentiation. DKMF did not show any inhibitory effect on the differentiation. The released Mg ions from the fibers were within the concentration range that supports differentiation. As the magnesium ions could inhibit the Wnt/β-Catenin signaling pathway, the suppression of osteogenic differentiation was expected.[63] A more recent study showed magnesium ions might support osteogenic differentiation in a dose-dependent manner by activating Notch signaling.[64] DKMF supports the osteogenic differentiation of mesenchymal stem cells by activating the Wnt/β-Catenin signaling pathway, inhibiting adipogenic and chondrogenic differentiation. With their limited effect on the Wnt signaling pathway, the magnesium ions also induce the expression of Notch1, which promotes osteogenic differentiation.

DKMF promotes large axonal sprouting and needle-like elongation of osteoblast cells on day 7 after seeding osteoblast cells in nanofibers. It can be explained that the extracellular matrix and its components influenced cell morphology and offered a suitable platform for successful axon growth and elongation supporting communication between cells and the microenvironment, triggering the process of bone tissue.

In vitro results showed that cells incubated on DKMF enhanced cellular functions such as migration, infiltration, proliferation, and differentiation. Osteoblast cells on DKMF surface showed a needle shape morphology with a multilateral cytoskeleton while the cells were spread

691 on the pure fiber surface by pseudopodia-like extended structures. The cell−matrix and cell-cell
692 interactions were demonstrated using SEM and confirmed by confocal microscopy observations.
693
694 **5. CONCLUSION**
695 The osteoinductive effect of DKMF produced by electrospinning was evaluated in this study.
696 PLA(TCP)/PCL composite ratio was optimized at 1:1 (v/v) concentration and APIs were loaded
697 in this ratio. The addition of APIs into composite slightly increased the diameter of electrospun
698 nanofibers, which could be attributed to a slight decrease in solution viscosity. The addition of
699 APIs to composite fibers slightly decreased Tm and Tg values, but there is no significant
700 difference in the operating temperature; it increased the tensile strength and made the structure of
701 scaffolds more proper by making them tougher and softer compared to pure fiber. The water up-
702 take capacity increased as enhancing of fiber diameter while the degradation ratio decreased.
703 Although all APIs (D_3, K_2, and Mg) were released in a sustained release manner for 144 h. Both
704 pure nanofiber and DKMF supported fibroblast cell viability. The cell death could not be
705 observed, but the cell growth was slightly decreased in both cultures of fibers. DKMF supported
706 the osteogenic differentiation of mesenchymal stem cells by activating the Wnt/β-Catenin
707 signaling pathway with the expression of Runx2, BMP2, and osteopontin and suppression of
708 PPAR-γ and Sox9. At the same time, DKMF suppressed the differentiation into adipogenic and
709 chondrogenic cells. Using confocal laser scanning microscopy after 7 days of incubation, DKMF
710 promoted large axonal sprouting and needle-like elongation of osteoblast cells and enhanced
711 cellular functions as migration, infiltration, proliferation, and differentiation. The results
712 confirmed that DKMF has the osteoinductive effect, and it is a promising treatment approach for
713 bone tissue engineering.
714 **CONFLICT OF INTEREST**
715 The authors have no competing interests.
716

ACKNOWLEDGEMENTS

Ece Guler and Yaren Ezgi Baripoglu contributed equally to this work.

REFERENCES

[1] I. Shirzaei Sani, M. Rezaei, A. Baradar Khoshfetrat, D. Razzaghi, Preparation and characterization of polycaprolactone/chitosan-g-polycaprolactone/hydroxyapatite electrospun nanocomposite scaffolds for bone tissue engineering, Int. J. Biol. Macromol. 182 (2021) 1638-1649.

[2] S. Ranganathan, K. Balagangadharan, N. Selvamurugan, Chitosan and gelatin-based electrospun fibers for bone tissue engineering, Int. J. Biol. Macromol. 133 (2019) 354-364.

[3] S.D. McCullen, Y. Zhu, S. Bernacki, R. Narayan, B. Pourdeyhimi, R. Gorga, E. Loboa, Electrospun composite poly (L-lactic acid)/tricalcium phosphate scaffolds induce proliferation and osteogenic differentiation of human adipose-derived stem cells, Biomed. Mater. 4 (2009) 035002.

[4] H. Alenezi, M.E. Cam, M. Edirisinghe, Experimental and theoretical investigation of the fluid behavior during polymeric fiber formation with and without pressure, Appl. Phys. Rev. 6 (2019) 041401.

[5] M.E. Cam, A.N. Hazar-Yavuz, S. Cesur, O. Ozkan, H. Alenezi, H. Turkoglu Sasmazel, M. Sayip Eroglu, F. Brako, J. Ahmed, L. Kabasakal, G. Ren, O. Gunduz, M. Edirisinghe, A novel treatment strategy for preterm birth: Intra-vaginal progesterone-loaded fibrous patches, Int. J. Pharm. 588 (2020) 119782.

[6] J. Xue, T. Wu, Y. Dai, Y. Xia, Electrospinning and Electrospun Nanofibers: Methods, Materials, and Applications, Chem. Rev. 119 (2019) 5298-5415.

[7] K.C. Castro, M.G.N. Campos, L.H.I. Mei, Hyaluronic acid electrospinning: Challenges, applications in wound dressings and new perspectives, Int. J. Biol. Macromol. 173 (2021) 251-266.

743 [8] M.E. Cam, S. Cesur, T. Taskin, G. Erdemir, D.S. Kuruca, Y.M. Sahin, L. Kabasakal, O.
744 Gunduz, Fabrication, characterization and fibroblast proliferative activity of electrospun Achillea
745 lycaonica-loaded nanofibrous mats, Eur. Poly. J. 120 (2019) 109239.
746 [9] J. Jeong, J.H. Kim, J.H. Shim, N.S. Hwang, C.Y. Heo, Bioactive calcium phosphate materials
747 and applications in bone regeneration, Biomater. Res. 23 (2019) 4.
748 [10] R. Dwivedi, S. Kumar, R. Pandey, A. Mahajan, D. Nandana, D.S. Katti, D. Mehrotra,
749 Polycaprolactone as biomaterial for bone scaffolds: Review of literature, J. Oral Biol. Craniofac.
750 Res. 10 (2020) 381-388.
751 [11] A. Abalymov, B. Parakhonskiy, A.G. Skirtach, Polymer- and Hybrid-Based Biomaterials
752 for Interstitial, Connective, Vascular, Nerve, Visceral and Musculoskeletal Tissue Engineering,
753 Polymers (Basel), 12 (2020).
754 [12] D.-H. Kim, C.A. Meza, H. Clarke, J.-S. Kim, R.C. Hickner, Vitamin D and Endothelial
755 Function, Nutrients, 12 (2020) 575.
756 [13] M. van Driel, J. van Leeuwen, Vitamin D endocrinology of bone mineralization, Mol. Cell
757 Endocrinol. 453 (2017) 46-51.
758 [14] G.B. Wasilewski, M.G. Vervloet, L.J. Schurgers, The Bone—Vasculature Axis: Calcium
759 Supplementation and the Role of Vitamin K, Front. Cardiovasc. Med. 6 (2019).
760 [15] M.A. Wsoo, S.I.A. Razak, S.P.M. Bohari, S. Shahir, R. Salihu, M.R.A. Kadir, N.H.M.
761 Nayan, Vitamin D3-loaded electrospun cellulose acetate/polycaprolactone nanofibers:
762 Characterization, in-vitro drug release and cytotoxicity studies, Int. J. Biol. Macromol. 181
763 (2021) 82-98.
764 [16] M. Halder, P. Petsophonsakul, A.C. Akbulut, A. Pavlic, F. Bohan, E. Anderson, K. Maresz,
765 R. Kramann, L. Schurgers, Vitamin K: Double Bonds beyond Coagulation Insights into
766 Differences between Vitamin K1 and K2 in Health and Disease, Int. J. Mol. Sci. 20 (2019) 896.
767 [17] V. di Giacomo, A. Cataldi, S. Sancilio, Biological Factors, Metals, and Biomaterials
768 Regulating Osteogenesis through Autophagy, Int. J. Mol. Sci. 21 (2020).

769 [18] N. Rijal, U. Adhikari, S. Khanal, D. Pai, J. Sankar, N. Bhattarai, Magnesium oxide-poly(ε-
770 caprolactone)-chitosan-based composite nanofiber for tissue engineering applications, Mater.
771 Sci. Eng. B 228 (2018) 18-27.
772 [19] C. Zhu, R. Cao, Y. Zhang, R. Chen, Metallic Ions Encapsulated in Electrospun Nanofiber
773 for Antibacterial and Angiogenesis Function to Promote Wound Repair, Front. Cell Dev. Biol. 9
774 (2021).
775 [20] G. Belgheisi, M.H. Nazarpak, M.S. Hashjin, Bone tissue engineering electrospun scaffolds
776 based on layered double hydroxides with the ability to release vitamin D3: Fabrication,
777 characterization and in vitro study, Appl. Clay Sci. 185 (2020) 105434.
778 [21] F.M. Salih, Effect of clothing varieties on solar photosynthesis of previtamin D3: an in vitro
779 study, Photodermatol. Photoimmunol. Photomed. 20 (2004) 53-58.
780 [22] L. Kim, K. Brudzynski, Identification of menaquinones (vitamin K2 homologues) as novel
781 constituents of honey, Food Chem. 249 (2018) 184-192.
782 [23] W. Chen, Cross-linked Chitosan in Mini-tablets for Controlled Drug Release, Citeseer
783 (2005).
784 [24] T. Ramezanli, B.E. Kilfoyle, Z. Zhang, B.B. Michniak-Kohn, Polymeric nanospheres for
785 topical delivery of vitamin D3, Int. J. Pharm. 516 (2017) 196-203.
786 [25] D. Wójcik-Pastuszka, J. Krzak, B. Macikowski, R. Berkowski, B. Osiński, W. Musiał,
787 Evaluation of the release kinetics of a pharmacologically active substance from model intra-
788 articular implants replacing the cruciate ligaments of the knee, Materials 12 (2019) 1202.
789 [26] A. Aydın, G. Duruksu, G. Erman, C. Subaşı, A. Aksoy, Z.S. Ünal, E. Karaöz, Neurogenic
790 differentiation capacity of subacromial bursal tissue—derived stem cells, J. Orthop. Res. 32
791 (2014) 151-158.
792 [27] R. Fang, E. Zhang, L. Xu, S. Wei, Electrospun PCL/PLA/HA based nanofibers as scaffold
793 for osteoblast-like cells, J. Nanosci. Nanotechnol. 10 (2010) 7747-7751.

794 [28] A. Alakrach, N. Noriman, O.S. Dahham, R. Hamzah, M.A. Alsaadi, Z. Shayfull, S.S. Idrus,
795 in: Journal of Physics: Conference Series, IOP Publishing, 2018, pp. 012065.
796 [29] B. Mehdikhani, G.H. Borhani, Densification and mechanical behavior of β-tricalcium
797 phosphate bioceramics, Int. Lett. Chem. Phys. Astron. 17 (2014).
798 [30] E.I. Nep, B.R. Conway, Preformulation studies on grewia gum as a formulation excipient, J.
799 Therm. Anal. Calorim. 108 (2012) 197-205.
800 [31] J.C. Bonor, R.J. Schaefer, N. Menegazzo, K. Booksh, A.G. Nohe, Design of 1, 25
801 dihydroxyvitamin D3 coupled quantum dots, a novel imaging tool, J. Nanosci. Nanotechnol. 12
802 (2012) 2185-2191.
803 [32] A.A. Bunaciu, E.G. Udriştioiu, H.Y. Aboul-Enein, X-ray diffraction: instrumentation and
804 applications, Crit. Rev. Anal. Chem. 45 (2015) 289-299.
805 [33] J.E. Oliveira, L.H. Mattoso, W.J. Orts, E.S. Medeiros, Structural and morphological
806 characterization of micro and nanofibers produced by electrospinning and solution blow
807 spinning: a comparative study, Adv. Mater. Sci. Eng. 2013 (2013).
808 [34] Y. Lu, Y.-C. Chen, P.-H. Zhang, Preparation and characterisation of polylactic acid
809 (PLA)/polycaprolactone (PCL) composite microfibre membranes, Fibres Text. East. Eur. (2016).
810 [35] Y.-C. Fu, C.-H. Chen, C.-Z. Wang, Y.-H. Wang, J.-K. Chang, G.-J. Wang, M.-L. Ho, C.-K.
811 Wang, Preparation of porous bioceramics using reverse thermo-responsive hydrogels in
812 combination with rhBMP-2 carriers: In vitro and in vivo evaluation, J. Mech. Behav. Biomed.
813 Mater. 27 (2013) 64-76.
814 [36] C. Aguzzi, P. Cerezo, I. Salcedo, R. Sánchez, C. Viseras, Mathematical models describing
815 drug release from biopolymeric delivery systems, Mater. Technol. 25 (2010) 205-211.
816 [37] V.I. Dos Santos, C. Merlini, Á. Aragones, K. Cesca, M.C. Fredel, In vitro evaluation of
817 bilayer membranes of PLGA/hydroxyapatite/β-tricalcium phosphate for guided bone
818 regeneration, Mater. Sci. Eng. C 112 (2020) 110849.

819 [38] A. Vieira, J. Vieira, J. Ferra, F. Magalhães, R. Guedes, A. Marques, Mechanical study of
820 PLA–PCL fibers during in vitro degradation, J. Mech. Behav. Biomed. Mater. 4 (2011) 451-460.
821 [39] F. Alexis, Factors affecting the degradation and drug‐release mechanism of poly (lactic
822 acid) and poly [(lactic acid)‐co‐(glycolic acid)], Polym. Int. 54 (2005) 36-46.
823 [40] S. Khan, N.M. Ranjha, Effect of degree of cross-linking on swelling and on drug release of
824 low viscous chitosan/poly (vinyl alcohol) hydrogels, Polym. Bull. 71 (2014) 2133-2158.
825 [41] Z. Xu, J. Li, H. Zhou, X. Jiang, C. Yang, F. Wang, Y. Pan, N. Li, X. Li, L. Shi,
826 Morphological and swelling behavior of cellulose nanofiber (CNF)/poly (vinyl alcohol)(PVA)
827 hydrogels: poly (ethylene glycol)(PEG) as porogen, RSC Adv. 6 (2016) 43626-43633.
828 [42] S. Tungprapa, T. Puangparn, M. Weerasombut, I. Jangchud, P. Fakum, S. Semongkhol, C.
829 Meechaisue, P. Supaphol, Electrospun cellulose acetate fibers: effect of solvent system on
830 morphology and fiber diameter, Cellulose 14 (2007) 563-575.
831 [43] F. Elshishiny, W. Mamdouh, Fabrication of Nanofibrous/Xerogel Layer-by-Layer
832 Biocomposite Scaffolds for Skin Tissue Regeneration: In Vitro Study, ACS Omega 5 (2020)
833 2133-2147.
834 [44] M. Ansari, Bone tissue regeneration: biology, strategies and interface studies, Progress in
835 Biomaterials 8 (2019) 223-237.
836 [45] E. Mariani, G. Lisignoli, R.M. Borzì, L. Pulsatelli, Biomaterials: Foreign Bodies or Tuners
837 for the Immune Response?, Int. J. Mol. Sci. 20 (2019) 636.
838 [46] S. Cesur, F.N. Oktar, N. Ekren, O. Kilic, D.B. Alkaya, S.A. Seyhan, Z.R. Ege, C.-C. Lin,
839 S.E. Kuruca, G. Erdemir, O. Gunduz, Preparation and characterization of electrospun polylactic
840 acid/sodium alginate/orange oyster shell composite nanofiber for biomedical application, J. Aust.
841 Ceram. Soc. (2019).
842 [47] M.E. Cam, S. Yildiz, H. Alenezi, S. Cesur, G.S. Ozcan, G. Erdemir, U. Edirisinghe, D.
843 Akakin, D.S. Kuruca, L. Kabasakal, O. Gunduz, M. Edirisinghe, Evaluation of burst release and

844 sustained release of pioglitazone-loaded fibrous mats on diabetic wound healing: an in vitro and
845 in vivo comparison study, J. R. Soc. Interface 17 (2020) 20190712.
846 [48] G. Fernandez de Grado, L. Keller, Y. Idoux-Gillet, Q. Wagner, A.-M. Musset, N.
847 Benkirane-Jessel, F. Bornert, D. Offner, Bone substitutes: a review of their characteristics,
848 clinical use, and perspectives for large bone defects management, J. Tissue Eng. 9 (2018)
849 2041731418776819-2041731418776819.
850 [49] S.D. McCullen, Y. Zhu, S.H. Bernacki, R.J. Narayan, B. Pourdeyhimi, R.E. Gorga, E.G.
851 Loboa, Electrospun composite poly(L-lactic acid)/tricalcium phosphate scaffolds induce
852 proliferation and osteogenic differentiation of human adipose-derived stem cells, Biomed. Mater.
853 4 (2009) 035002.
854 [50] M. Diba, W.A. Camargo, M. Brindisi, K. Farbod, A. Klymov, S. Schmidt, M.J. Harrington,
855 L. Draghi, A.R. Boccaccini, J.A. Jansen, J.J.J.P. van den Beucken, S.C.G. Leeuwenburgh,
856 Composite Colloidal Gels Made of Bisphosphonate-Functionalized Gelatin and Bioactive Glass
857 Particles for Regeneration of Osteoporotic Bone Defects, Adv. Funct. Mater. 27 (2017) 1703438.
858 [51] M.E. Cam, B. Ertas, H. Alenezi, A.N. Hazar-Yavuz, S. Cesur, G.S. Ozcan, C. Ekentok, E.
859 Guler, C. Katsakouli, Z. Demirbas, D. Akakin, M.S. Eroglu, L. Kabasakal, O. Gunduz, M.
860 Edirisinghe, Accelerated diabetic wound healing by topical application of combination oral
861 antidiabetic agents-loaded nanofibrous scaffolds: An in vitro and in vivo evaluation study,
862 Mater. Sci. Eng. C 119 (2021) 111586.
863 [52] S.-F. Chou, K.A. Woodrow, Relationships between mechanical properties and drug release
864 from electrospun fibers of PCL and PLGA blends, J. Mech. Behav. Biomed. Mater. 65 (2017)
865 724-733.
866 [53] Y.H. Kim, D.W. Kim, M.S. Kwon, K.H. Cho, J.O. Kim, C.S. Yong, H.G. Choi, Clopidogrel
867 Napadisilate Monohydrate Loaded Surface-Modified Solid Dispersion: Physicochemical
868 Characterization and in Vivo Evaluation, Biol. Pharm. Bull. 38 (2015) 1033-1040.

869 [54] K.J. Rambhia, P.X. Ma, Controlled drug release for tissue engineering, J. Control. Release.
870 219 (2015) 119-128.
871 [55] J. López-García, M. Lehocký, P. Humpolíček, P. Sáha, HaCaT Keratinocytes Response on
872 Antimicrobial Atelocollagen Substrates: Extent of Cytotoxicity, Cell Viability and Proliferation,
873 J. Funct. Biomater. 5 (2014) 43-57.
874 [56] Y.-c. Shi, L. Worton, L. Esteban, P. Baldock, C. Fong, J.A. Eisman, E.M. Gardiner, Effects
875 of continuous activation of vitamin D and Wnt response pathways on osteoblastic proliferation
876 and differentiation, Bone 41 (2007) 87-96.
877 [57] Y.-R. Lou, T.C. Toh, Y.H. Tee, H. Yu, 25-Hydroxyvitamin D 3 induces osteogenic
878 differentiation of human mesenchymal stem cells, Sci. Rep. 7 (2017) 1-12.
879 [58] G.M. Boland, G. Perkins, D.J. Hall, R.S. Tuan, Wnt 3a promotes proliferation and
880 suppresses osteogenic differentiation of adult human mesenchymal stem cells, J. Cell. Biochem.
881 93 (2004) 1210-1230.
882 [59] T.F. Day, X. Guo, L. Garrett-Beal, Y. Yang, Wnt/β-catenin signaling in mesenchymal
883 progenitors controls osteoblast and chondrocyte differentiation during vertebrate skeletogenesis,
884 Dev. Cell 8 (2005) 739-750.
885 [60] K. Yonemura, M. Kimura, T. Miyaji, A. Hishida, Short-term effect of vitamin K
886 administration on prednisolone-induced loss of bone mineral density in patients with chronic
887 glomerulonephritis, Calcif. Tissue Int. 66 (2000) 123-128.
888 [61] M.J. Jeon, J.A. Kim, S.H. Kwon, S.W. Kim, K.S. Park, S.-W. Park, S.Y. Kim, C.S. Shin,
889 Activation of peroxisome proliferator-activated receptor-γ inhibits the Runx2-mediated
890 transcription of osteocalcin in osteoblasts, J. Biol. Chem. 278 (2003) 23270-23277.
891 [62] S. Castiglioni, V. Romeo, L. Locatelli, A. Cazzaniga, J.A. Maier, TRPM7 and MagT1 in the
892 osteogenic differentiation of human mesenchymal stem cells in vitro, Sci. Rep. 8 (2018) 1-10.
893 [63] A.M. de Oca, F. Guerrero, J.M. Martinez-Moreno, J.A. Madueno, C. Herencia, A. Peralta,
894 Y. Almaden, I. Lopez, E. Aguilera-Tejero, K. Gundlach, Magnesium inhibits Wnt/β-catenin

activity and reverses the osteogenic transformation of vascular smooth muscle cells, PloS One 9 (2014) e89525.

[64] J.M. Díaz-Tocados, C. Herencia, J.M. Martínez-Moreno, A.M. de Oca, M.E. Rodríguez-Ortiz, N. Vergara, A. Blanco, S. Steppan, Y. Almadén, M. Rodríguez, Magnesium Chloride promotes Osteogenesis through Notch signaling activation and expansion of Mesenchymal Stem Cells, Sci. Rep. 7 (2017) 1-12.